Università
Ca'Foscari
Venezia

Master's Degree
in Science and
Technology of Bio
and Nano materials

High-efficiency luminescent solar concentrators based on eco-friendly carbon Dots Fluorophores

Supervisors
Prof. Kassa Belay Ibrahim
Prof. Elisa Moretti

Student
Jodi Gobbo
855035

Academic Year
2023 / 2024

Acronyms

CA: citric acid

CDs: carbon quantum dots

Em: emission

EROI: energy return on energy investment

EtOH: ethanol

Ex: excitation

FTIR: Fourier transform infrared

HRTEM: high resolution transmission electron microscope

I-V: current-voltage

LSC: luminescent solar concentrator

MetOH: methanol

PCE: photon conversion efficiency

PLA: polylactic acid

PV: photovoltaic

PVP: polyvinyl pyrrolidone

QY: quantum yield

TRPL: time resolved photoluminescence

UV: ultra-violet

XRD: X-ray diffraction

Contents

Abstract

Nowadays environmental pollution deriving from energy production for human consumption has led to a huge demand for energy produced from renewable sources to reduce the human footprint on the environment. One of the most exploited renewable energy sources is solar light, which can be collected by photovoltaic (PV) cells to produce current. Most PV cells are made of silicon, which is not transparent to visible light. Consequently, silicon PV cells cannot be installed on windows, and this confines their application to roofs of buildings. Moreover, achieving high solar-to-electrical power conversion efficiency (PCE) at a low cost remains a challenge for solar cells. A solution to these problems can be the installation of luminescent solar concentrators (LSCs) on windows, which allow most of the visible light to pass through while UV light is absorbed, transformed into visible light thanks to photoluminescence effect and guided toward a PV cell that can use it to produce energy. To achieve high-efficiency LSCs, it is crucial to synthesize fluorophores with excellent optical properties, such as broad absorption spectrum, high quantum yield (QY), and good stability. Carbon quantum dots (CDs) are a type of fluorophores that offer advantages such as a wide absorption spectrum, high quantum yield, non-toxicity, environmental friendliness, low cost, and eco-friendly synthesis methods. However, CDs have a relatively small Stokes shift compared to inorganic quantum dots, which limits their external optical efficiency. In this study CDs were synthesized and used for fabrication of high-efficiency LSCs. The synthesis method utilizes a facile and scalable hot plate approach to prepare CDs, which are then characterized using various techniques, including X-ray diffraction (XRD), high-resolution transmission electron microscopy (HRTEM), UV-Vis absorption spectroscopy, and photoluminescence spectroscopy. The LSCs were later coupled to a silicon PV cell to check their efficiency via I-V curve tests. The synthesized CDs resulted to have two size populations of respectively 13±2 nm and 22±2 and a QY of 75.9% when dispersed in ethanol. The CDs based LSCs resulted to have an absorption peak centered at 406 nm, an emission peak centered at 530 nm, a Stokes shift of 0.71 eV and a QY of 60.8%. These findings have potential applications in various fields, including building-integrated photovoltaics, solar windows, and wearable devices. Further optimization of the doping concentration and synthesis parameters could lead to even higher performance of the CDs in LSCs, paving the way for their practical

implementation in next-generation solar energy harvesting devices. For the characterization of LSCs with I-V curve, an instrument that aimed to connect a solar simulator, the LSCs, a PV cell and the instrument for the I-V test was design, 3D printed and successfully used for the measurements with the intention to standardize the I-V curve measurements for further studies on LSCs both at Ca'Foscari University and in other research institutions.

1. Introduction

1.1.Population growth and Energy consumption

In the past centuries human population has constantly increase and, according to trends, it might exceed 10 billion of people within the 2100 [1–3]. Due to population growth and improvement of life standards, world energy consumption is increasing. This is happening because energy consumption is related to both number of Earth's inhabitants and human wellbeing, which are following a positive trend in accordance with recent studies [4]. Over the past years, energy production has led to a huge environmental cost in terms of pollution, in fact, it is one of the main causes of the emission of greenhouse gasses in the atmosphere. Moreover, the production of energy is also related to other environmental problems such as particulate emission, soil overexploitation, drought and water pollution [5,6]. Among the most discussed greenhouse gasses there is carbon dioxide (CO_2) [7], which daily reaches concentrations around 420 ppm according to the Mauna Loa Observatory (Hawaii) **Figure 1**.

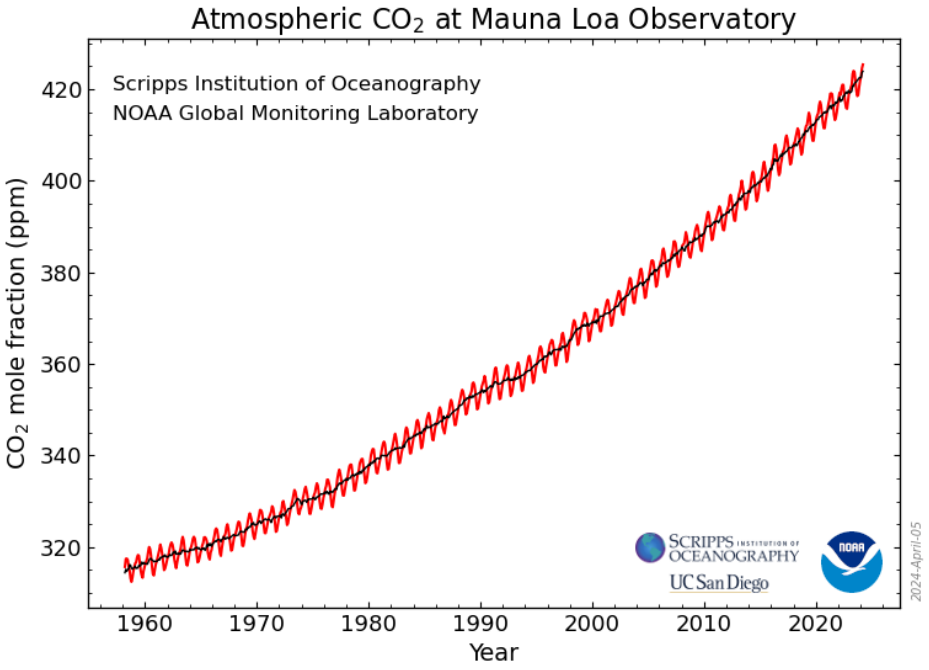

Figure 1 *The graph shows monthly mean CO_2 concentration measured at Mauna Loa Observatory, Hawaii. The carbon dioxide data on Mauna Loa constitutes the longest record of direct measurements of CO_2 in the atmosphere.* [8]

As reported in the figure, CO_2 concentration has never stop growing in the last sixty years[9]. Since the first studies on environmental pollution in the 60s, many efforts have been made to make the energy production processes more independent from non-renewable sources, however, carbon and oil contributions to energy production are still predominant, as reported in **Figure 2**.

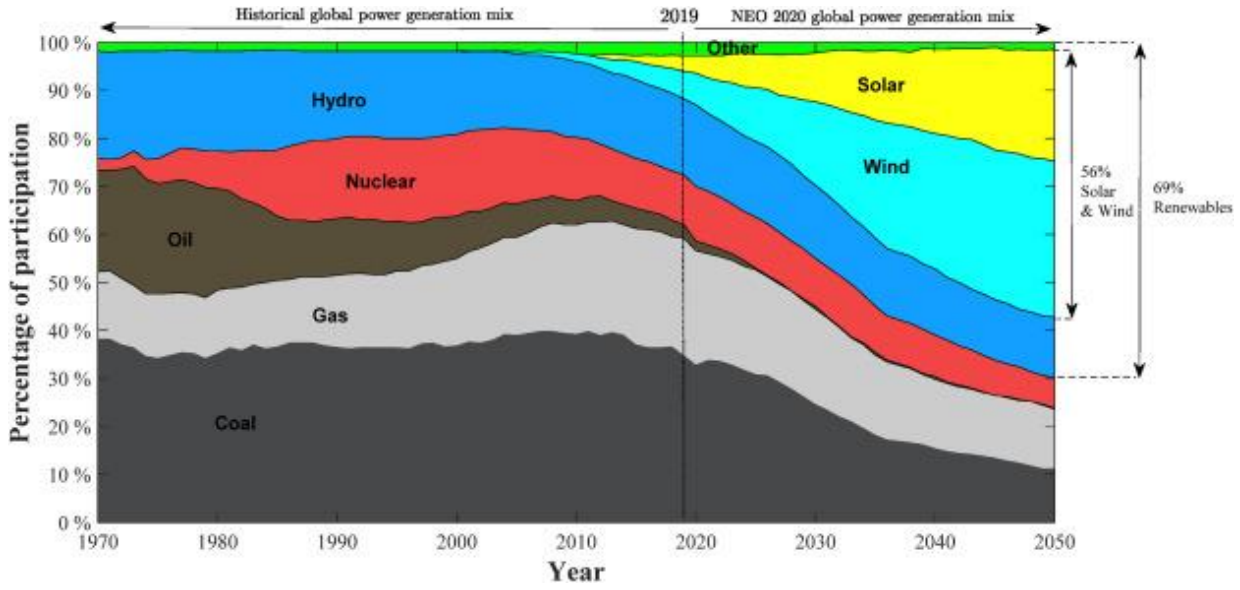

***Figure 2**: global electricity sources from 1970 up to 2050* [10]

In the figure are also reported predictions on future trends of renewable sources exploitation, which are supposed to reach the 50% of the total world energy production within thirty years. Nowadays, thanks to new technologies, it is possible to count on a wide number of renewable energy sources. This is of crucial importance because any energy source has its own limitations and there is no source that is perfect for human utilization[11]. These is the main reason why there is the need for differentiation and combination of energy sources to guarantee a constant energy supply to the whole human population in every part of the world. At the same time, there is the necessity to decrease human impact on the environment to preserve the planet for future generations [12,13]. However, a low impact on the environment is just one of the many parameters that a renewable energy source must accomplish to be considered a valid alternative to conventional fossil fuels.

The ideal renewable source should be abundant, continuous, constant, never-ending, well distributed, safe, non-polluting, easily exploitable, easily storable, easily transportable, concentrated, unlimited, renewable, economically affordable to everyone, it should not generate inequalities between the users and, of course, it should have a low environmental impact. A parameter that must be taken into account when investing in a renewable source is the Energy Return on Energy Invested (EROI) index, which gives an estimation on how convenient it is to invest in an energy source in terms of energy, before this source starts to pay back the energy that was required to activate it [14,15]. As written above, among all the existing and known renewable sources, there is no one that has all the characteristics cited above to be considered "perfect" [16], and this is why there is the need for a differentiation of the energy sources. Wind energy and energy from biomasses, for example, are not continuous, they require a lot of soil consumption, and they are not exploitable in every region of the world[17,18]. Consequently, they need to be coupled with other sources to guarantee a constant energy supply. For the development of the new technologies that are needed to maximize the exploitation of a certain energy source, it is important to first estimate what is potential of that source. In **Figure 3** it is reported an estimation on how much the most common renewable sources are exploited in comparison with how much these sources can offer in terms of energy (image of 2011).

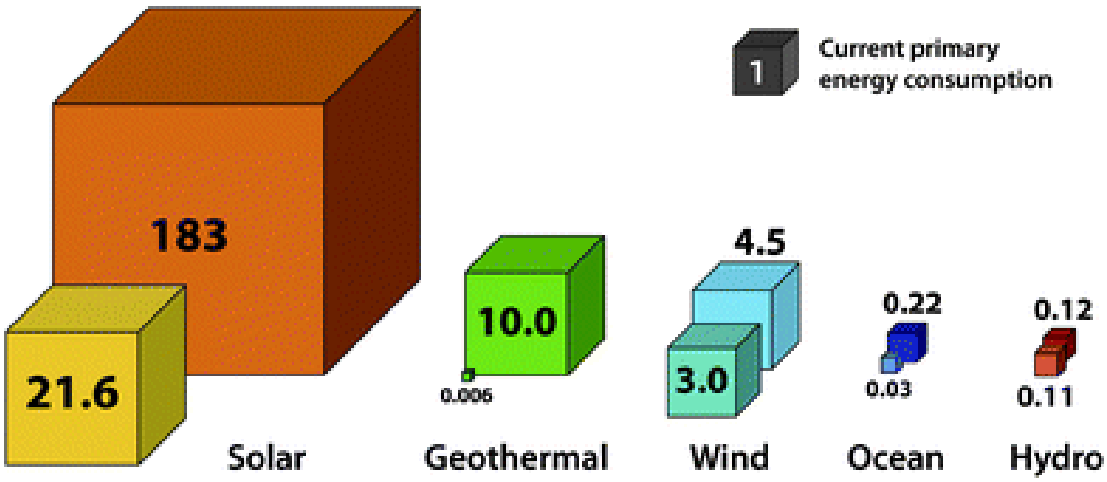

Figure 3 *Schematic representation of the relative amounts of potentially available (large cubes) and technically exploitable (small cubes) renewable energies, compared to the current primary energy consumption (dark grey)* [19]

The figure gives a rough idea of the potential of renewable sources; however, this data can deviate from reality due to development of new technologies for a more efficient exploitation of these energy sources. For example, its probably not convenient to invest in new technologies for hydroelectric since we almost reached the maximum possible exploitation of this source. Moreover, hydroelectric has been used for many decades[20] and it is an already well known source. Therefore, it is unlikely that new technologies will consistently improve its exploitation. On the contrary, solar energy (in particular photovoltaic) is relatively recent if compared to other sources[21]. Therefore, it can offer further developments thanks to new technologies like highly efficient photovoltaic cells [22,23] or luminescent solar concentrators that are the focus of this study.

1.2. Solar energy

Among all existing renewable sources, solar energy seems to be one of the most interesting since it has many of the characteristics of the ideal source that were reported above. In fact, it is abundant, never-ending, well distributed and available all over the world, safe, unlimited, economically affordable, it does not require expensive technologies and it is easily storable with batteries. The main problems with solar energy are basically two, the first one is that it is not continuous and constant in time, the second one is that it requires a high area to furnish enough energy for human consumption. It is not possible to precisely estimate the minimum area of PV cells that a person needs to be energetically independent from other sources because energy consumption pro capita depends on many factors such as age, gender, lifestyle and socio-economic parameters of a person [24,25]. It is claimed that an average solar cell that is to be found on the market can produce between 250 and 450 W/h [26–28]. If we imagine to install a PV plant with 15 PV cells on the roof of a house, we can estimate a minimum daily energy production of about 30 kW/h (since 250 W/h * 8 hours * 15 PV cells = 30 kW/h), which would be more than enough to cover the energetic demand per capita in the majority of the countries in the world[29–31]. PV cells are normally installed on roofs of buildings instead of on walls because direct solar illumination guarantees a better efficiency of the cells. Due to the high costs of the most common silicon PV cells, it is normally not convenient to install them on vertical surfaces because their productivity would not be high enough to justify their installation in terms of costs and energy demand for their fabrication. This is a huge limitation because all the walls of buildings that are

illuminated by solar light are currently not exploited solar energy production. Nowadays there are some materials for solar energy harvesting that are cheaper than silicon as in the case of organic low-cost PV cells[32,33]. However, they tend to be less stable and less efficient if compared with inorganic PV cells, even if progresses have been made in recent years[34,35]. Furthermore, PV cells demonstrate low transparency to visible light, which means that they cannot be applied on windows since they will stop the light from entering buildings and provide natural illumination.

1.3.Luminescent Solar Concentrators (LSCs)

As discussed above, it would not be convenient to cover buildings walls with PV cells due to their high costs. A solution to this problem might be the application of Luminescent Solar Concentrators (LSCs) on buildings windows. LSCs are fluorescent optical guidelines that can collect the light impinging on their surface and concentrate it on their edges thanks to total internal reflection principle[36] **Figure 4(a)**. An LSC can then be coupled with one or more PV cells that will be placed at its edges as represented in **Figure 4(b)**. In this way, the PV cell can use the light outcoming from the LSC edge to produce energy.

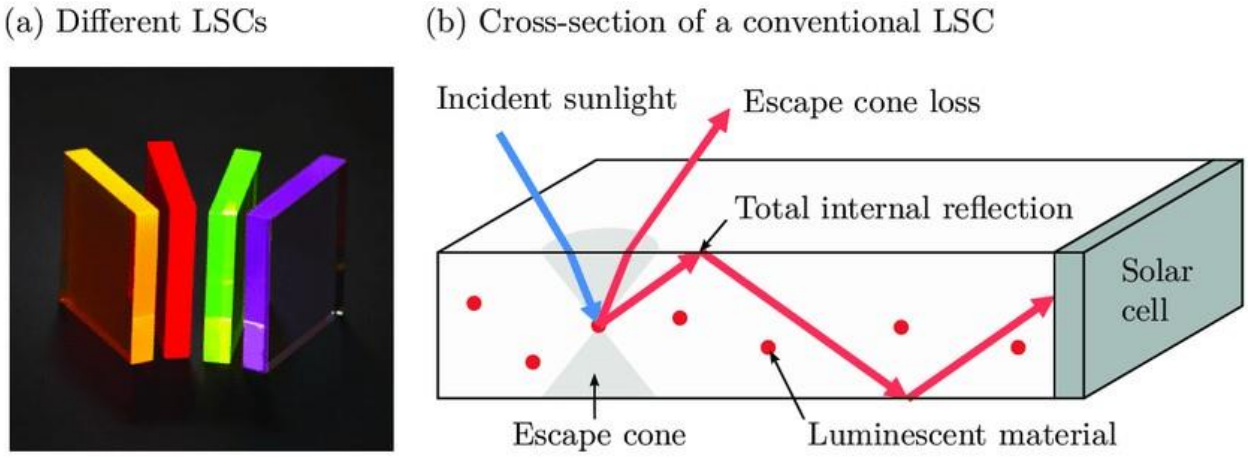

Figure 4 (a) *LSCs with different colors and* ***(b)*** *Working principle of an LSCs: the fluorophore molecule act as an emitting center: it absorbs light and it reemits it at a different wavelength, the emitted photons are directed toward the edges of the LSCs by total internal reflection* [37]

One of the main advantages of this technology is that it requires small area PV cells in comparison to conventional PV plants. In this way, the costs of energy plants can be drastically reduced. Furthermore, LSCs contain fluorophores that cause light to be absorbed and emitted

back at lower frequency due to non-radiative relaxation phenomena **Figure 5**. Every fluorophore molecule or particle present in the LSC can be considered as a light emitting center.

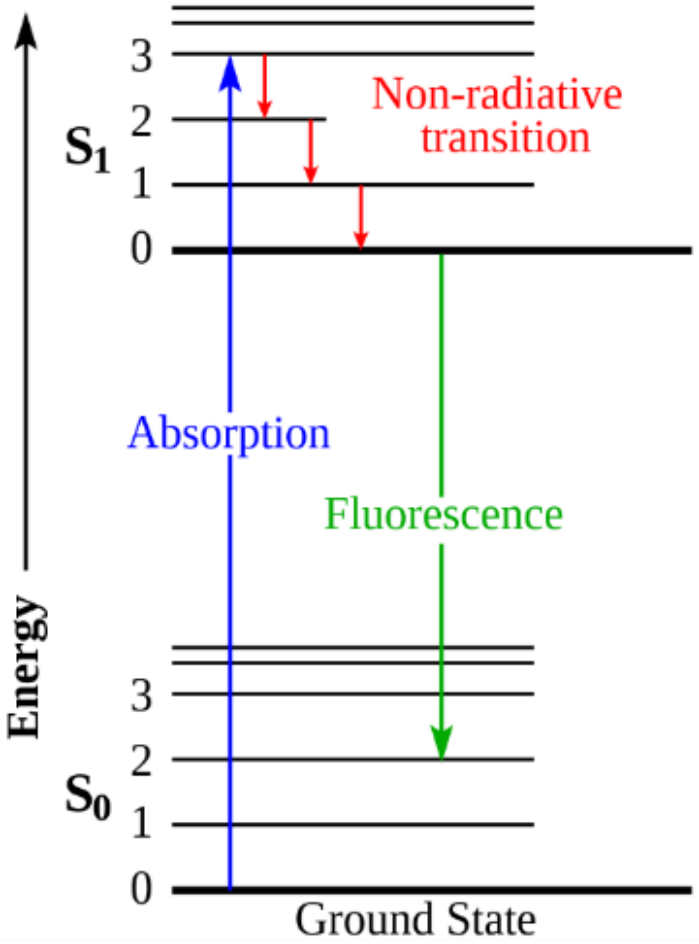

Figure 5 *Fluorescence working principle: an electron is excited to another energy level by a photon, it loses some energy non-radiatively and goes back to its original energy level emitting a photon with lower frequency.* [38]

The working principle of a fluorophore is called fluorescence, and it consist in the absorption of a photon by the fluorophore, which causes an excitation of an electron of the valence band of the fluorophore (S0 in the figure) to an excited energy state in the conduction band. Subsequently, the electron loses part of its energy by non-radiative emission until it reaches the lower energy level of the conduction band. From this energy level, the electron can finally go back to the valence band through radiative emission. This last step results in an emission of a photon with an energy lower than the energy of the photon that was absorbed. Thanks to fluorescence,

fluorophores allow LSCs to transform UV light into visible light and this is of great importance for PV energy production. In fact, the majority of PV cells that can be found on the market guarantee a better efficiency when illuminated by visible light instead of UV light[39]. The best wavelengths for an optimal efficiency of a PV cell can be determined by measuring the spectral response of the PV cell[40,41]. In **Figure 6** are reported the spectral response of four commercial PV cells under solar spectrum illumination.

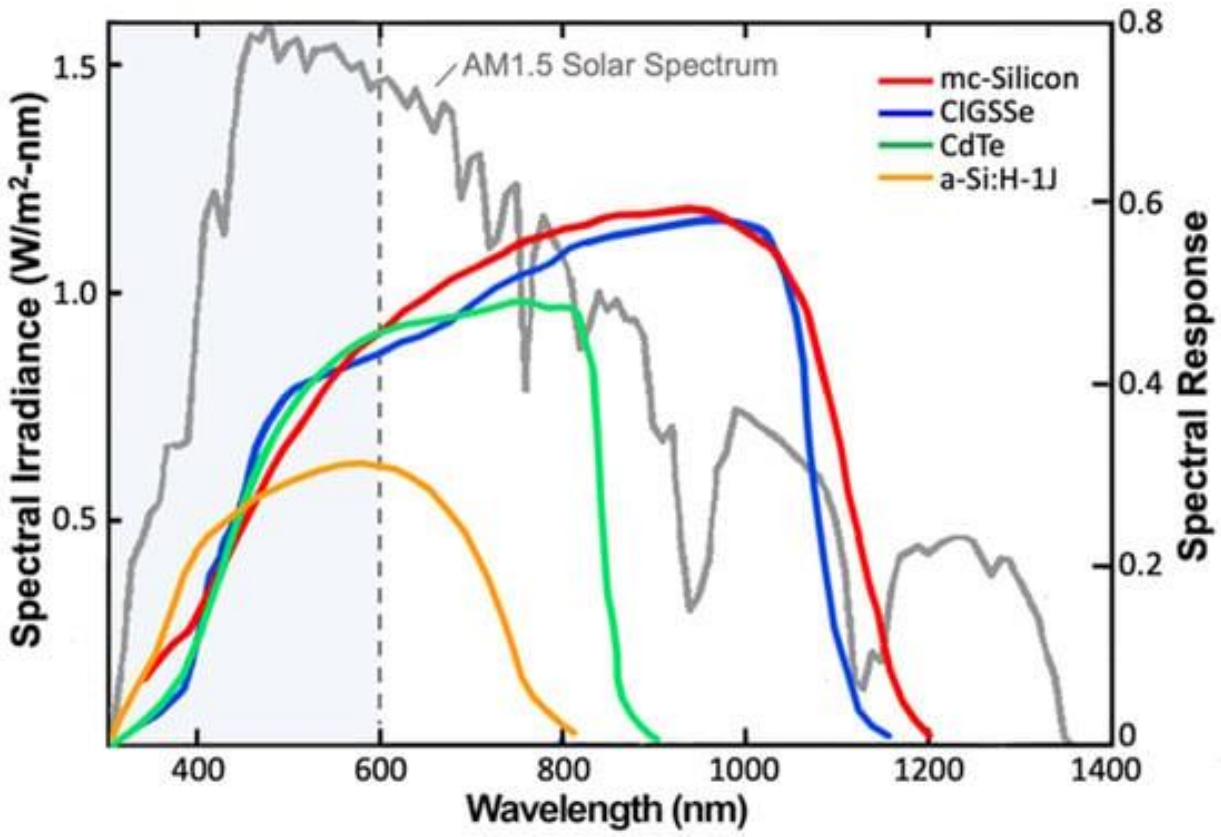

Figure 6 *Spectral response comparisons of four commercial PV modules (c-Si, CdTe, CIGS, and a-Si:H) indicating responses in various spectral regions compared to AM1.5 solar spectrum*

As shown in the picture, the spectral response peaks for all four PV cells tested are far from UV region, which confirms that PV cells have low efficiency under UV irradiation. The coupling of a PV cell with an LSC will allow to produce energy from UV light, which would not possible for a PV cell operating under direct solar illumination and this is the reason why LSCs have great potential in PV energy applications. Furthermore, LSCs have other important advantages, first, their absorption spectrum can be easily tuned according to their chemical composition[42].

Secondly, they are highly transparent to visible light, which makes them suitable for installation on windows to provide natural illumination. Moreover, LSCs absorb highly energetic light that is harmful for the human body[43], preventing against skin cancer. There are different types of LSCs according to their structure and chemical composition[44,45]. Normally the fluorophore is embedded in a matrix; while the fluorophore is responsible for the fluorescence, the matrix gives the structure of the LSC and acts as a light guideline, concentrating at the edges the light emitted by the fluorophore. The emission of fluorophore in an LSC should ideally resemble the spectrum that guarantees the best efficiency of the PV cell mounted on its edges. This spectrum varies according to the type of PV cell used, as it was reported in **Figure 6**. It is possible to design an LSC such that its emission fits the peak of the spectral response of the PV cell. In this way the efficiency of the LSC-PV system will be optimized. This result can be obtained selecting the right fluorophores for the LSC according to their emission spectrum. Ideally a fluorophore for LSCs should absorb a broad spectrum of UV light and emit with a narrow emission spectrum with the peak centered at the most suitable wavelength for the coupled PV cell. A phenomenon that can decrease the efficiency of LSCs is photon reabsorption, which occurs when an emitting center absorbs a photon that was emitted by another emitting center due to overlap of absorption and emission spectra of the fluorophore[46] **Figure 7**. To overcome this problem, fluorophores can be engineered in order increase the gap between their absorption and emission peaks, which is called Stokes shift. This result can be obtained with different strategies like the doping of the fluorophore [47,48].

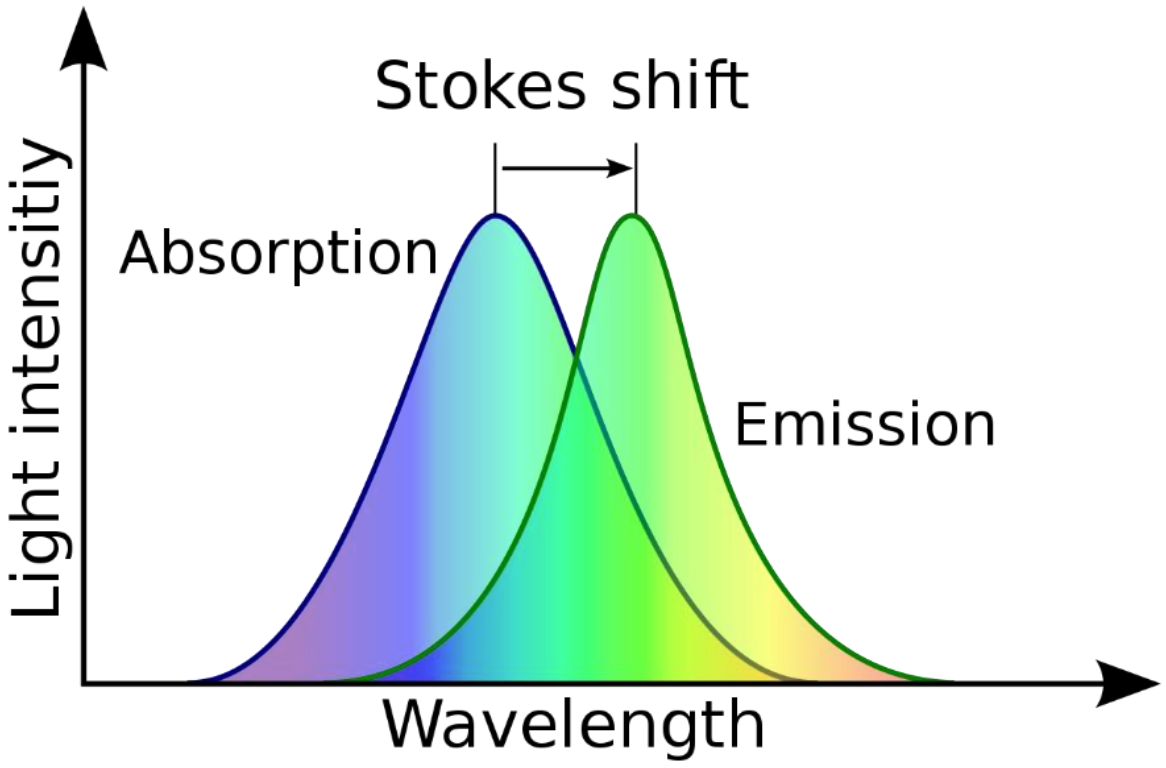

Figure 7*: Stokes shift representation (gap between absorption and emission peaks). The photons in the central overlapped region are those that can be reabsorbed after being emitted by the fluorophore.* [49]

It must be considered that a too wide Stokes shift can also have a negative influence on the efficiency of the LSCs because a wide Stokes shift is obtained by increasing the non-radiative emission of the fluorophore, which means that part of the energy absorbed by the fluorophore will be lost in heat of the LSC. Due to this energy loss, the total radiative energy emitted by LSC edges will be lower than the total energy collected by the LSC surface. In the case of large area LSCs, it is also crucial to have a low photon reabsorption because light must travel a long distance inside the LSC before reaching the edges. If the photon path is long, it will be more likely for the photon to interact with an emitting center that might reabsorb, this can decrease the number of photons reaching the PV cell at the edge of the LSC.

1.4. CDs as Fluorophores

In this study, high efficiency LSCs were produced using carbon dots (CDs) as fluorophores. CDs are normally spherical shaped particles made of pure carbon that show fluorescence[50]. They can

be synthesized with different methods and they have many possible applications in different fields such as medicine, environment and spectroscopy[51]. Here the CDs for the LSCs were synthesized with a hotplate using urea, citric acid (CA) and $CaCl_2$ as precursors. CDs tend to have a broad emission spectrum if compared with inorganic fluorophores due to their electronic complexity. This is not ideal for PV applications because the broader the LSC emission is, the further will it be from the PV spectral response peak, which leads to a decrease of PV efficiency. On the other hand, CDs have many other advantages, they can be easily doped, functionalized or decorated to have higher stability or to optimize their optical features [52–54]. For instance, modifications can change the shape and position of CDs absorption and emission peaks or they can broader both the CDs bandgap and Stokes shift. Moreover, precursors for CDs are commonly cheap, easily available, non-toxic, environment friendly and they can be obtained from organic wastes of industry or agricultural production processes[55–57]. The synthesis method used in this study resulted in being reproducible, fast (about two hours) and safe. The matrix that was chosen to embed the CDs is made of polyvinyl pyrrolidone (PVP) because it is transparent to most of the light absorbed and emitted by CDs and because its synthesis is quick and easy. PVP is also safe[58] and environment friendly[59] as in the case of CDs. For the assembling of LSCs, different LSCs designs were experimented, from simple drop casting of the CDs on the glass substrate to the sandwich design in which the CDs were enclosed between two glasses. This last design allows to protect CDs and PVP from direct exposure to atmospheric agents that might degrade them.

1.5. Black box design and fabrication

To determine the optical and physical characteristics of LSCs, different instruments are needed. While XRD, TEM and optical microscope were used on LSCs to confirm their chemical composition and the structure of CDs, UV-Vis and photoluminescence (PL) were fundamental to determine their optical characteristics, like their absorption and emission spectra and the Stokes shift. However, some complementary characterizations were needed to have an estimation of LSCs efficiency. Other analyses were therefore performed such as quantum yield (QY) and time resolved photoluminescence (TRPL). While QY aims to determine the ratio between the number of photons emitted and absorbed by the LSCs, the TRPL was used to estimate the average time

decay of the excited electrons. All these characterization techniques can give some estimations on the efficiency of the LSCs, but other experimental analyses are needed to determine how LSCs affect the PV cell productivity. The idea was to measure the I-V curve on the PV cell as it was coupled with the LSC. During this experiment, the LSC was illuminated by a solar simulator to simulate the outdoor conditions, at the same time, the instrument Keithley was connected to the PV cell to perform the I-V curve measurements. For this experiment it was needed a device to connect the solar simulator, the LSC, the PV cell and the Keithley instrument. A new device was therefore designed, 3D printed and successfully tested. This device basically consists of two joined obscure chambers, the first one with an opening for the solar simulator bulb and a shelf for the LSC, the second one with a holder for the PV cell, which is connected to Keithley.

2. Materials and methods

2.1. Materials

2.1.1. For CDs synthesis, purification and storage

Citric Acid (CA) purchased from Sigma-Aldrich, (>99.5%), urea, calcium dichloride ($CaCl_2$) from Sigma Aldrich, deionized water, ethanol absolute (>99.7%) that was purchased from VWR chemicals, silica gel, 100 ml beaker, Erlenmeyer flask, hotplate and magnetic stirrers, Pasteur pipette, UV torch 395 nm, bath sonicator, centrifuge for falcon tubes, falcon tubes, fridge and a glass filtering column with a fused silica quartz filter.

2.1.2. For PVP preparation

polyvinylpyrrolidone K30 from Thermo Fisher Scientific, polyvinylpyrrolidone K 90 (C_6H_9NO) from Sigma-Aldrich-Life Sciences (Switzerland), methanol from Sigma-Aldrich- Life Sciences (France), hotplate, magnetic stirrer, falcon tubes.

2.1.3. For LSCs synthesis and storage

PVP, CDs dispersed in ethanol, optical microscope slides, glass cutter, micropipette, hair dryer.

2.1.4. For optical characterization of CDs in liquid and for LSCs

for Uv-Vis analyses it was used a Cary Series UV-Vis-NIR Spectrophotometer Cary 5000, QY and TRPL measurements were performed with FLS980 Series Fluorescence Spectrometers (Edinburgh Instruments). For QY the instrument was equipped with an integrating sphere and the sample was excited with the wavelength that ensured the maximum emission. TRPL was measured exciting the sample with a picosecond pulsed diode laser EPL-375 (Edinburgh Instruments). For optical microscopy it was used an optical microscope 100 x.

2.1.5. For structural characterization of LSCs

for Transmission Electron Microscopy (TEM) characterization it was used a JEM-2100 F TEM (JEOL, Japan), X-Ray Diffraction was performed with a PW1050/37 diffractometer (Philips, Netherlands).

2.1.6. For volt-amperometric measurements of LSCs

to perform current-voltage measurements it was used a solar simulator (10500, Abet Technologies, Inc., Milford, CT, USA), a silicon PV cell and the instrument Keithley 2410. To connect the solar simulator, the LSCs, the PV cell and Keithley it was used a device that consists in a black box with two chambers. The box was designed, and 3D printed at Ca'Foscari University laboratories.

2.1.7. black box fabrication

3D printer Creality Ender S1 Pro, PLA black filament 1.75 mm thick (Creality CR-PETG).

2.2. Methods

Summary of the synthesis process of CDs LSCs

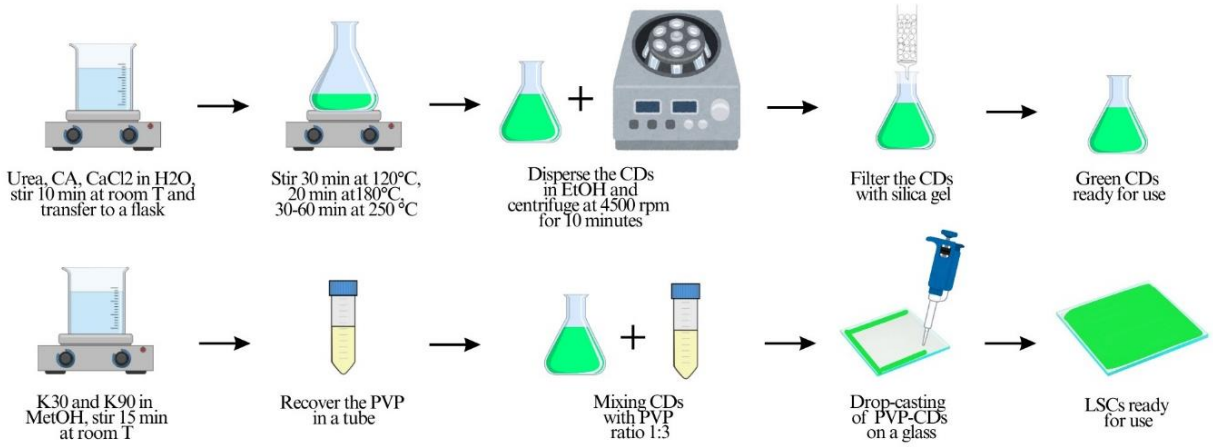

2.2.1. CDs synthesis, purification and storage

1.5 g of citric acid, 3 g of urea and 1 g of calcium dichloride ($CaCl_2$) were weighed and dissolved in a 100 ml beaker while vigorous stirring with a magnetic stirrer at room temperature. After 10 minutes, the solution that looked transparent and homogeneous **Figure 8(a)** was transferred into a 250 ml Erlenmeyer flask on a hotplate. The solution was stirred at 120°C for 30 minutes. In the

subsequent step, the temperature was increased up to 180° C keeping the same stirring. After 20 minutes, for the last step, the temperature was increased up to 250°C and kept constant for a time within half an hour and one hour, the time changed according to the type of hotplate and according to both the thickness and the shape of the flask. To decide when to stop the synthesis, it is better to rely on the color of the solution instead of on the time passed from the temperature increase. In the step at 250 °C, the solution changed its color, becoming yellowish and viscous **Figure 8(b)**. Normally a yellow-brown color indicates the formation of the first CDs. The solution was kept at 250°C and the stirring was increased with the increase of the viscosity of the solution to maintain the stirring regular. The solution changed in color from yellow to light brown and later it got darker and thicker to reach a brown color. At this stage, due to the high evaporation rate and the increase in viscosity, the solution changed into a colloid. As the synthesis went on, the color of the colloid changed into brown **Figure 8(c)**.

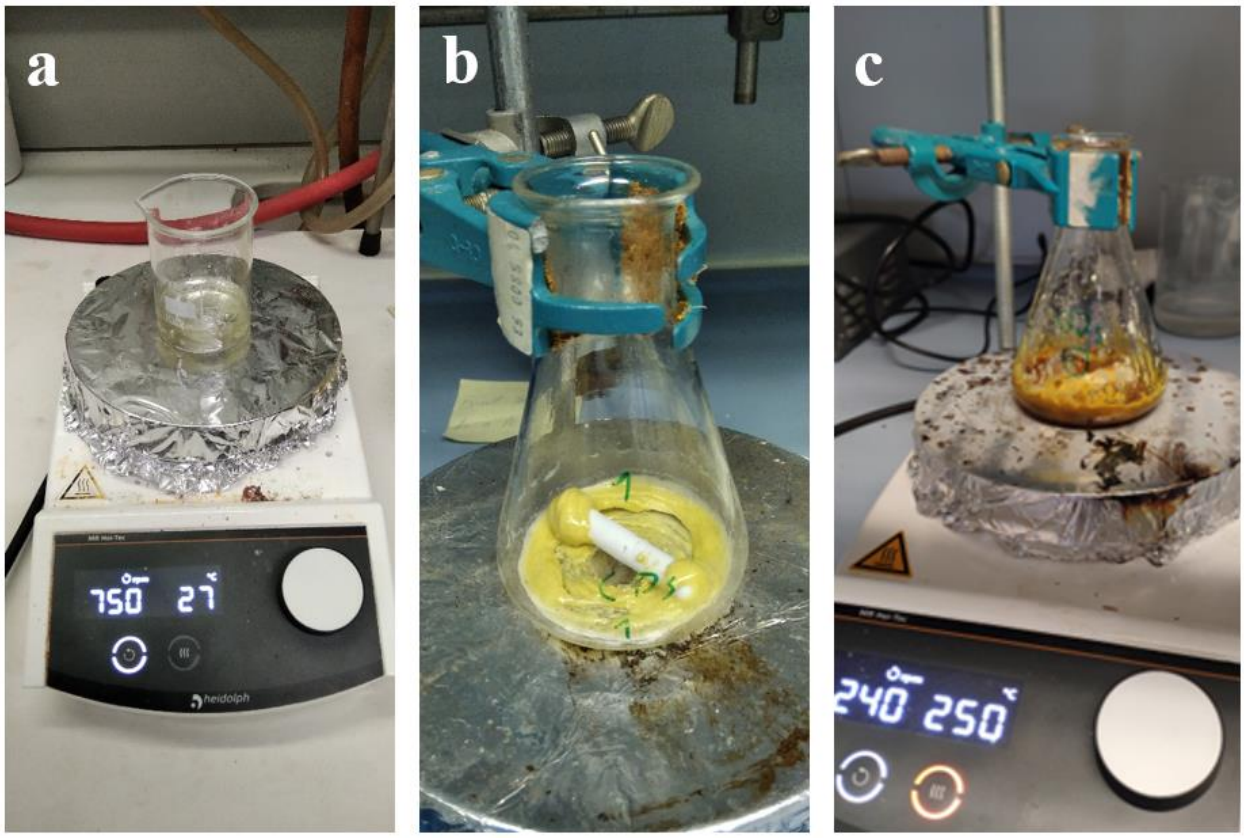

Figure 8 (a) *CA, urea and $CaCl_2$ in H_2O at room temperature,* ***(b)*** *formation of CDs,* ***(c)*** *CDs at the end of the synthesis process*

The formation of CDs during the synthesis was tested withdrawing a small amount of the colloid with a spatula every 5-10 minutes and dispersing it into a small beaker with ethanol. A UV torch (394 nm) was used to check the presence of CDs at different stages of the synthesis. The CDs dispersed in ethanol showed a bright green color due to their fluorescence when illuminated by the UV torch. The intensity of the fluorescence changed according to the stage of the synthesis: at early stages, fluorescence intensity was low, and it increased gradually as the synthesis process of CDs was at its last stages **Figure 9(a-e)**. At the last stage of the synthesis, the magnetic stirrer struggles to rotate, and the synthesis must be stopped adding ethanol to the flask to disperse the CDs **Figure 9(f)**. In some cases, the intensity of CDs fluorescence was so high that it was possible to see it even under solar light irradiation, without pointing the UV torch on the sample, in this case, a slight tilt of the flask can help enhancing the fluorescence effect **Figure 9(g)**.

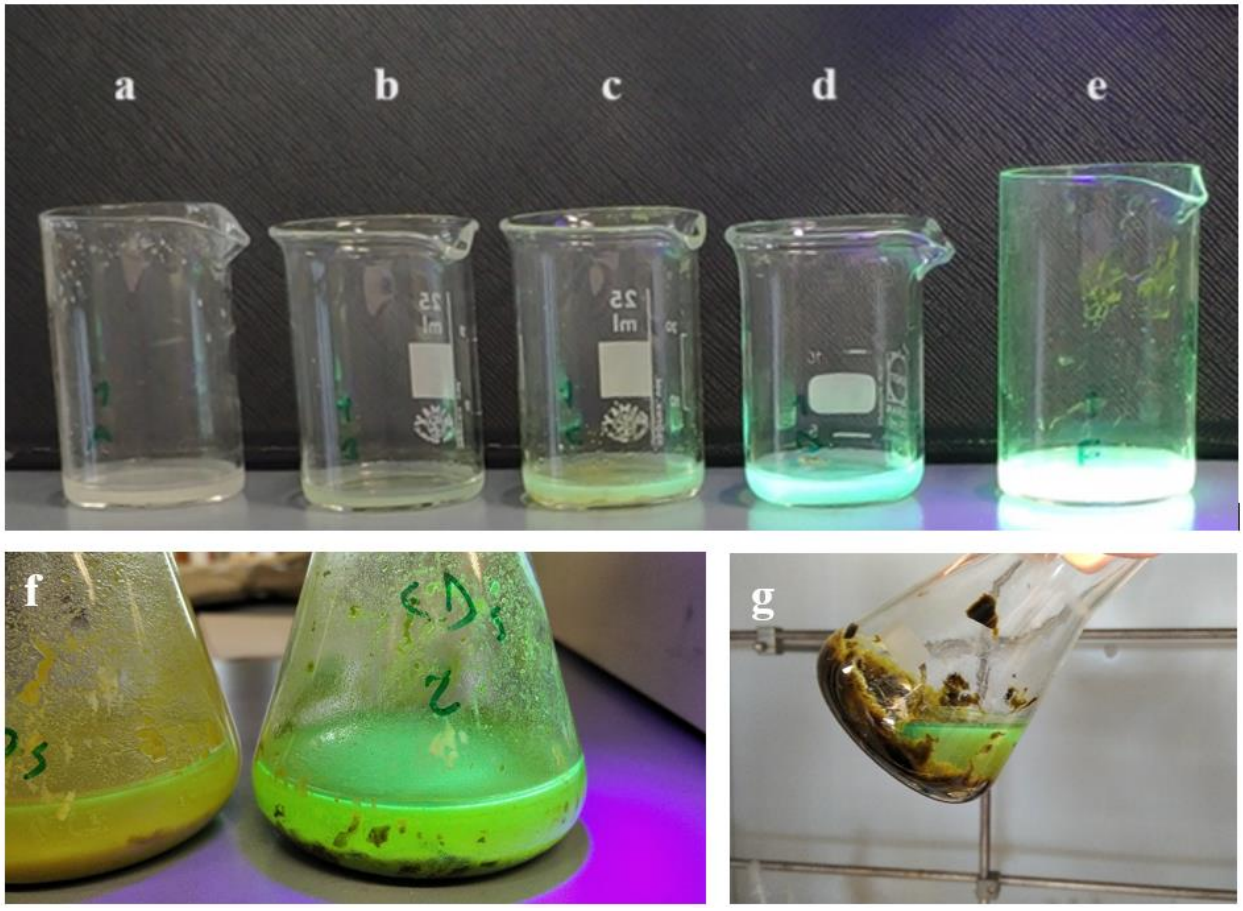

Figure 9 (a-e): *CDs withdrawn at different stages of the synthesis and dispersed in ethanol under UV light,* ***(f)****CDs at the end of the synthesis under UV light and* ***(g)*** *under solar light*

The UV torch method to check CDs fluorescence intensity is not a very reliable one but it can give a rough estimation on when to stop the reaction. The flask with CDs dispersed in ethanol was then put in a bath sonicator for 10 minutes to ensure an efficient dispersion of the CDs. The obtained solution was then put in a falcon tube and centrifuged at 4500 RPM for 10 minutes to sediment synthesis byproducts. After centrifugation, the CDs solution resulted to have a yellow color with a brown deposition at the bottom of the falcon tube **Figure 10(a)**. The solution was then transferred into a second falcon tube by fast pouring to avoid the brown precipitate detaching from the bottom of the first falcon tube. After this step the CDs were either directly used or preserved in a fridge to avoid their exposition to solar light which might enhance their degradation.

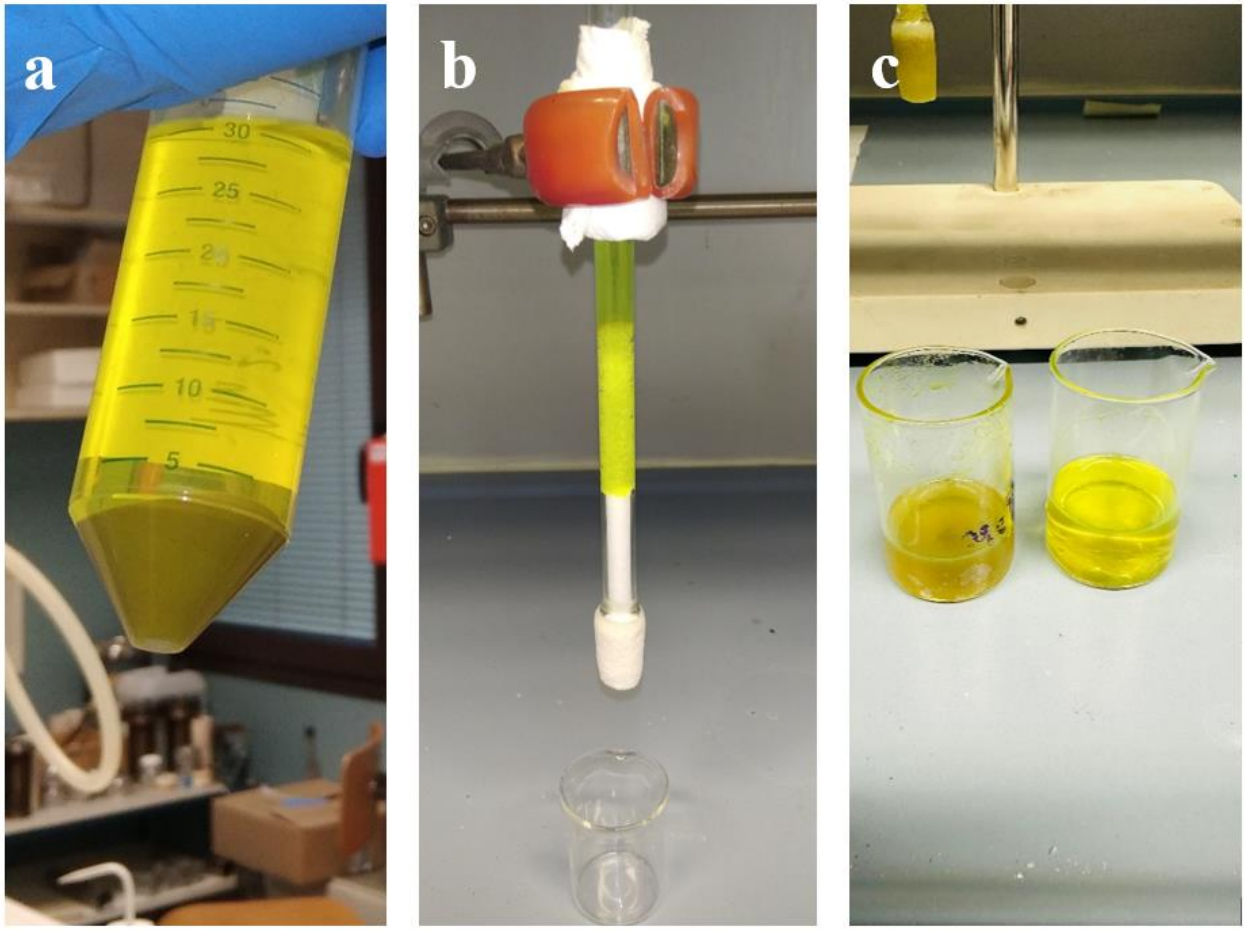

Figure 10 (a) *CDs in ethanol after centrifugation,* ***(b)*** *filtration of CDs with silica column,* ***(c)*** *CDs before (left) and after filtration*

A further purification process was successfully experimented, the CDs solution was filtered with a glass filtering column filled with silica gel up to about ¾ of its length. The column was first washed with methanol and then used for CDs filtration **Figure 10(b)**. After filtration the color of the CDs solution resulted in being brighter **Figure 10(c)**.

2.2.2. PVP preparation

1.5 g of K30 and 1.5 g of K90 per dissolved in a beaker with 15 ml of methanol under vigorous magnetic stirring at room temperature for 10 minutes. The PVP was then put in a falcon tube and preserved at room temperature.

2.2.3. LSCs fabrication

The glass substrate was prepared by cutting an optical microscope glass slide into three equal square glasses 2.5 x 2.5 cm **Figure 11(a)** with a glass cutter. The glasses were then washed with soap, acetone and dried with a piece of paper. The glass was then cleaned a second time with an air jet to the glass from any paper residue, which can cause a defect in the LSCs. The PVP solution was mixed with the CDs dispersed in ethanol in a small beaker with magnetic stirrer at room temperature with a ratio of PVP/CDs 3:1 and a second one of 1:1. The PVP-CDs solution was then drop-casted on the glass substrate with a micropipette **Figure 11(b)** and let dry for few hours. Different PVP-CDs amounts were tested such as 0.5 ml, 0.7 ml and 1 ml. To speed the drying process up, it was used an hair-drier. A similar procedure to the one already described was used to produce a large area LSCs of 4 cm x 4 cm **Figure 11(c)**, the amount of PVP-CDs solution used in this case was 2 ml**.** Finally, an LSCs with a sandwich structure was fabricated following the procedure used for the normal LSCs but after the drop-casting of the PVP-CDs layer, a second glass was deposited on the top of the LSC **Figure 11(d)**. The sandwich LSC was then let dry as in the case for the normal LSCs Figure.

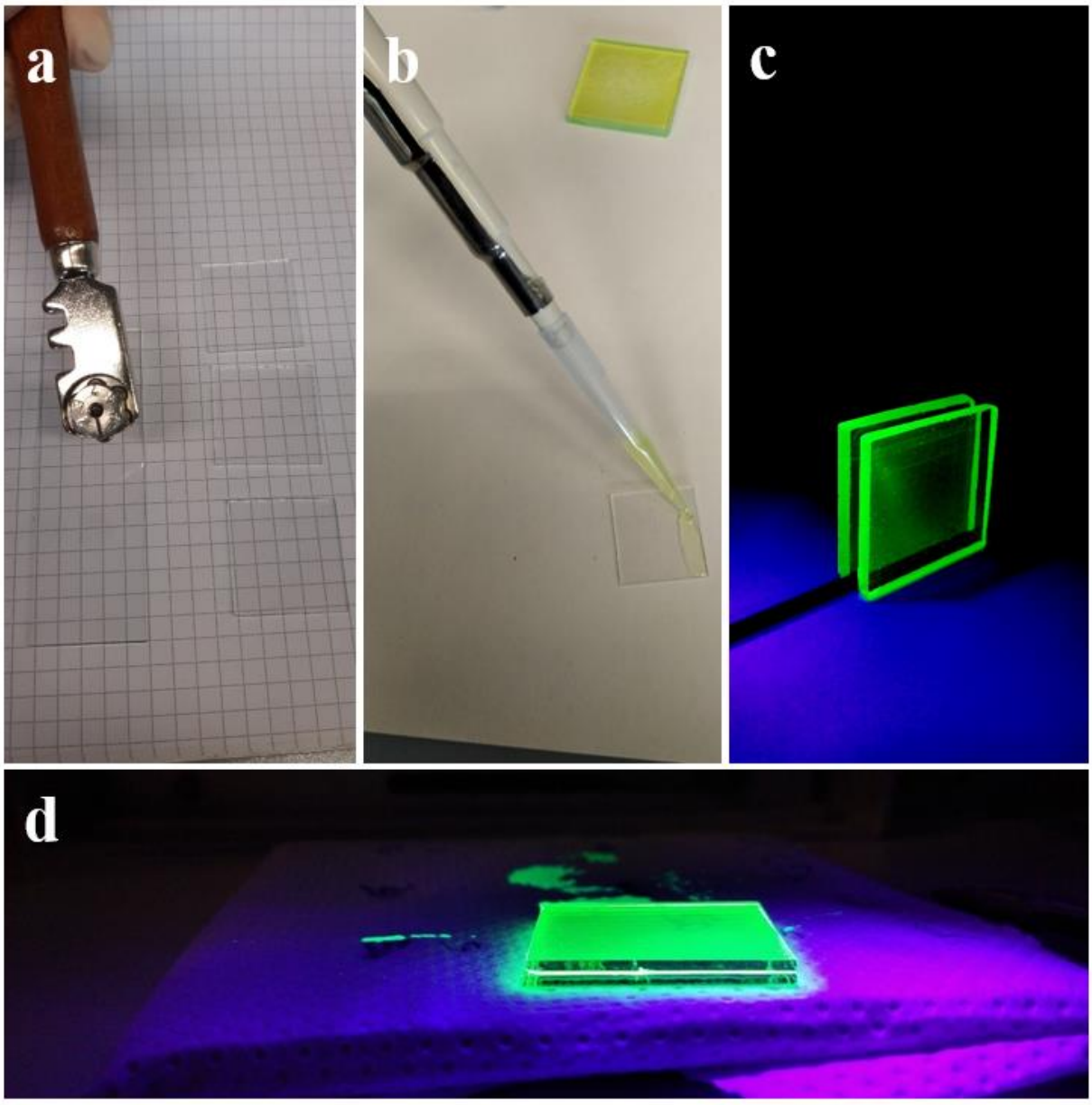

Figure 11 (a) *microscope slide cutting,* ***(b)*** *drop-casting of PVP-CDs layer on a glass slide,* ***(c)*** *large area LSCs under UV light,* ***(d)*** *sandwich LSCs under UV light*

2.2.4. Black box device for current-voltage LSCs characterization

The first version of the black box was hand-designed and then fabricated with cardboard **Figure 12(a).** After some tests of the black box, a second one was designed on AutoCAD and 3D printed in PLA **Figure 12(b)**. A PV cell was then integrated in the device and connected with clips to Keithley for the current-voltage measurements. **Figure 12(c)**.

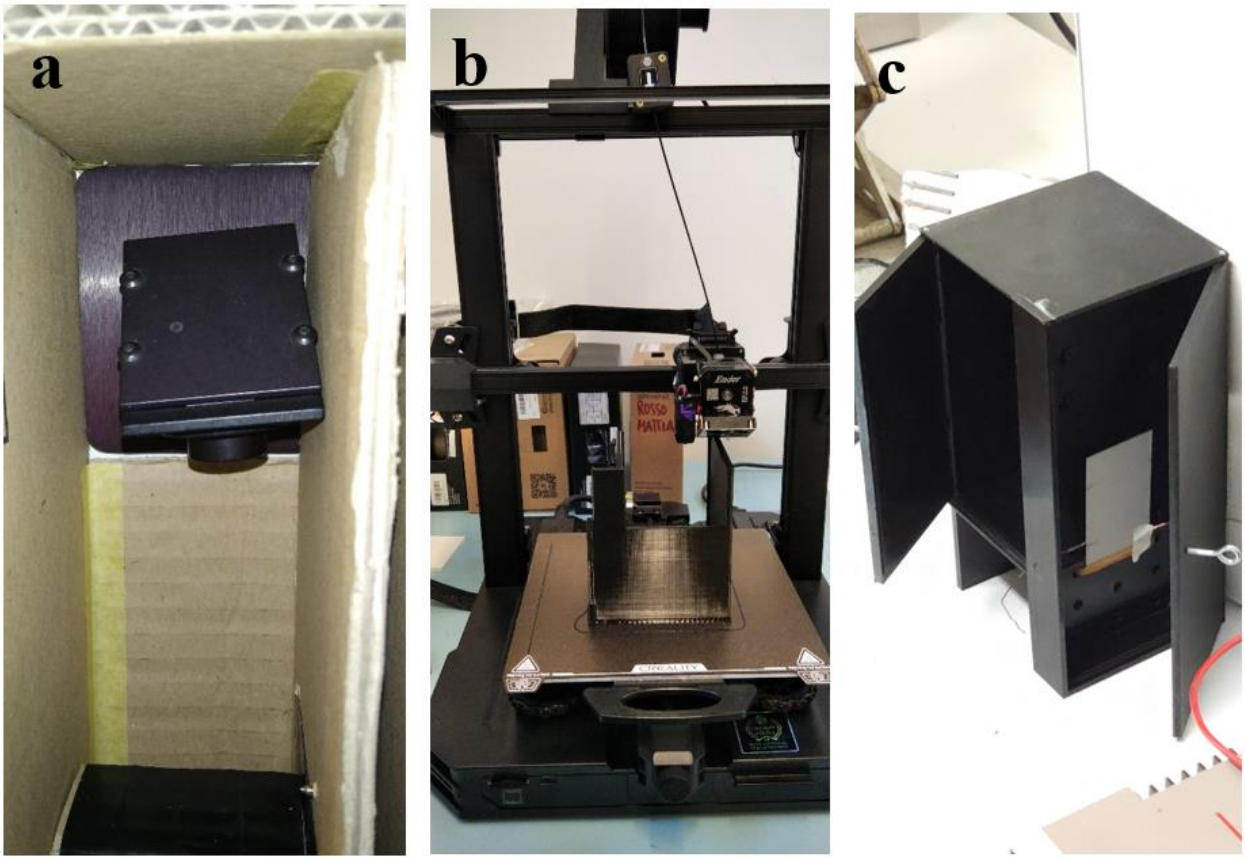

Figure 12 (a) *First black box,* ***(b)*** *3D printing of second black box,* ***(c)*** *final version of 3D printed black box*

2.2.5 Optical Characterization

2.2.5.1 UV-Vis characterization

absorption spectra were recorded for LSCs, for CDs in ethanol and for PVP-CDs solutions. The last two were recorded using a two-path instrument set up with 0.5 ml quartz cuvettes (cuvette optical path: 1 cm). The cuvette for the blank was filled with pure ethanol in the case of CDs dispersed in ethanol and a solution of PVP and ethanol in the case of the PVP-CDs solution.

2.2.5.2 PL characterization

First a PL emission mapping was recorded on the LSCs to determine the best excitation and emission wavelengths for the LSC. The PL emission spectrum was then recorded exciting the samples with the best excitation wavelength that was chosen according to the previous PL

mapping. Subsequently, the PL emission was performed a second time exciting the LSCs at 375 nm, which is a wavelength near to that of the laser that was used in TRPL measurements (372 nm). The aim of this second measurement was to use the same wavelength for PL and TRPL such that the data of these two measurements could be compared.

3.2.5.3 QY characterization

The measurements were performed on the LSCs using an integrating sphere and exciting the sample at 405 nm which was the best excitation wavelength according to the absorption spectrum recorded before.

2.2.6 Current-Voltage measurements

The I-V curve of the samples was obtained irradiating with a solar simulator the LSC that was coupled with a silicon PV cell. The PV cell was placed at one of the edges of the LSC. The solar simulator, the LSCs and the PV cell were kept at fixed positions for all the measurement thanks to the black box, in such way all the measurements were performed in the same conditions and the result obtained from different LSCs could be compared. The PV cell was connected to Keithley through two metal clips. Keithley was connected to a PC in which it was running the program LabTracer 2.0 for data collection. The set-up used for the measurements was the following:

Start voltage: 0
Stop voltage: 1.2
Number of points: 80
Compliance: 1
Sweep delay: 3
Filter count: 20

3. Results and discussion

3.1 Structural characterization

3.1.2 HRTEM characterization

HRTEM analyses confirmed the correct synthesis of the CDs as visible in **Figure 13(a)** and **13(b)**. The nanoparticles result in having a round shape and a diameter of tens of nanometers. As visible in **Figure 13(a)**, the size distribution of the CDs is not uniform, the average diameter was measured directly from the picture by summing all the diameters of randomly selected CDs and dividing the result by the number of CDs measured, the diameter resulted to be 19 ± 8 nm. However, it is clearly visible that there are at least two size populations. These findings were confirmed by statistical analyses performed on the collected data as follows: the data were plotted with Origin and analyzed with Gaussian fitting **Figure 14**. The first population shows an average diameter of 13 ± 2 nm and an R squared of 0.96.

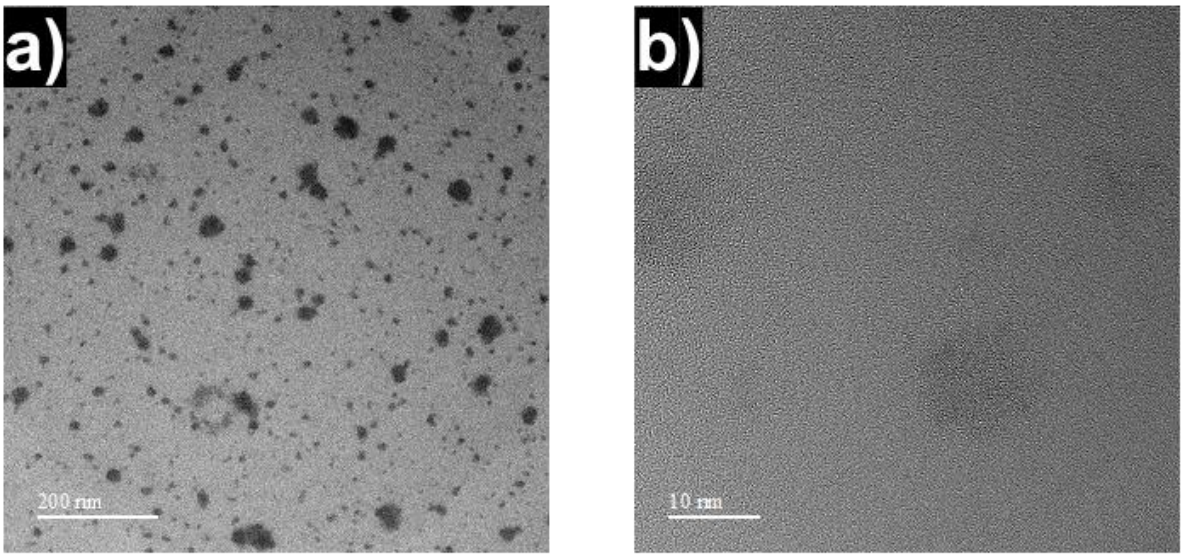

Figure 13 (a) *and* ***(b)*** *HRTEM images of the CDs*

In terms of number of particles, this population of CDs is apparently the biggest one of the three that were individuated by the Gaussian fitting. The second population has a diameter of 22 ± 2 nm with an R squared of 0.67. Finally, the last population shows a diameter of 34 ± 0.2 nm but due to its negative R squared, this data cannot be considered reliable. The CDs belonging to the third size population might have formed simultaneously with the smaller CDs or in later stages

of the synthesis due to agglomeration of smaller CDs or due to Oswald ripening. A way to determine which one of these assumptions is correct would be to withdraw a small amount of solution from which CDs are forming at different steps of the synthesis process and to analyze them with HRTEM to observe CDs formation and ripening.

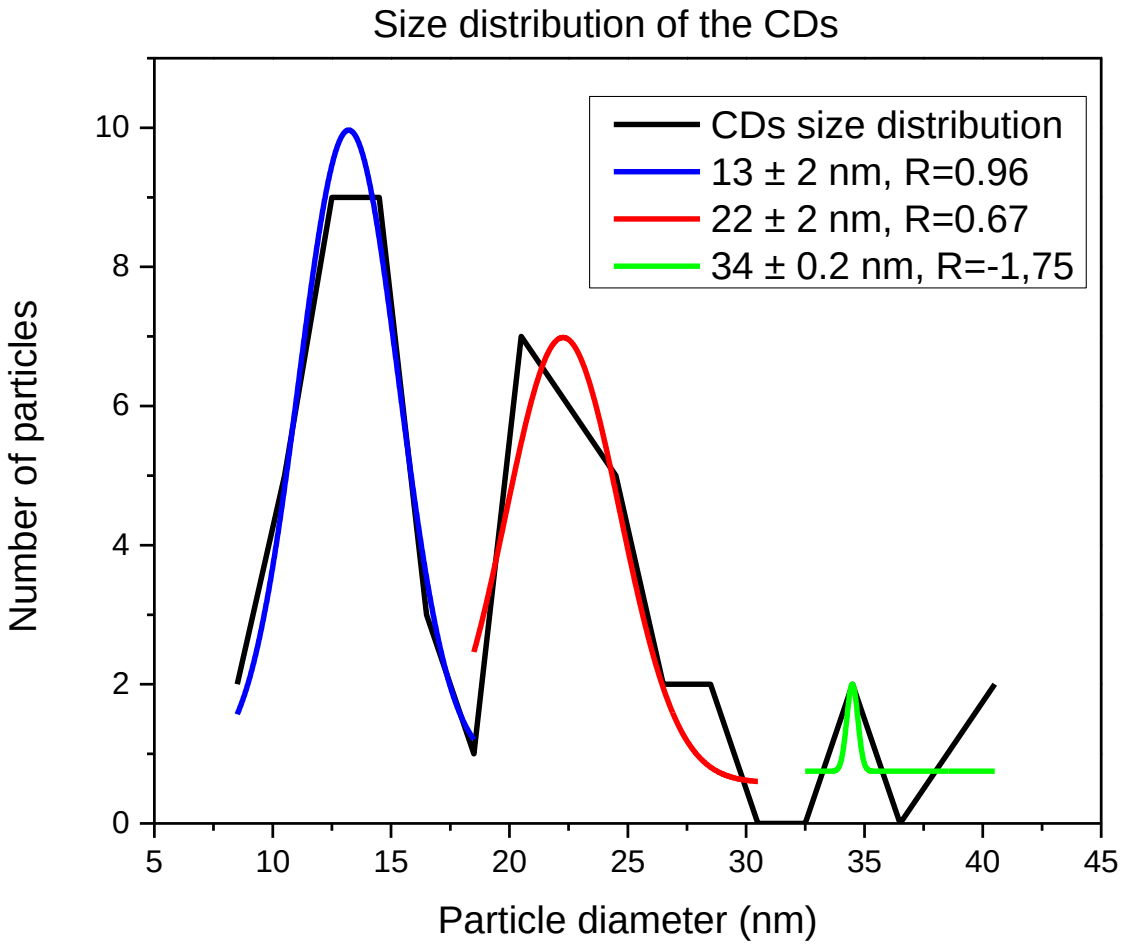

***Figure 14**: Gaussian fitting (blue, red and green lines) applied on the three size populations of CDs observed with HRTEM*

3.1.3 XRD and FTIR

According to XRD characterization, the CDs show two main peaks respectively at angles of 29 and 43 2θ **Figure 15(a)**. The second peak can be related to the 100 plane of graphene and the first one to the 002 plane. The XRD is compared with an XRD of graphene found in the literature[60] that is reported in **Figure 15(b).** The two XRD analyses result in being very similar, showing the two main peaks in the same positions. The sample was also analyzed with FTIR **Figure 15(c)**, where the bands deriving from -OH, N-H, C=O and C-O-C can be easily

recognized. The FTIR spectrum is compared with an FTIR performed on Ni-CDs that was found in the literature[61] **Figure 15(d)**. Since there is a good overlap of the peaks of the two spectra, it can be assumed that the two samples have a very similar composition.

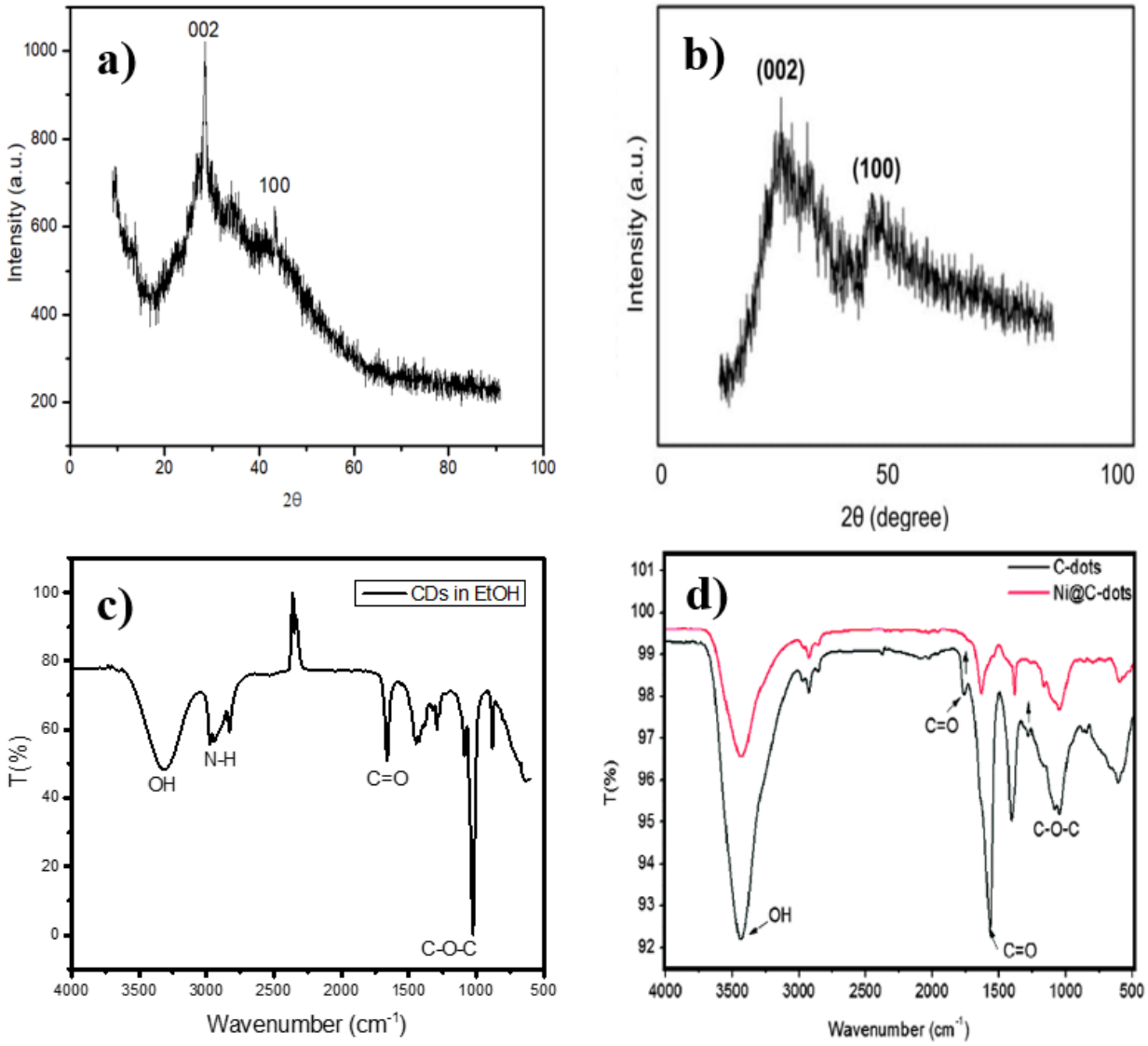

Figure 15 (a) *XRD of synthesized CDs,* ***(b)*** *XRD of graphene found in the literature,* ***(c)*** *FTIR of synthesized CDs and* ***(d)*** *FTIR of CDs found in the literature*

3.2 Optical characterization

3.2.1 Optical microscope analyses

After the first analyses with UV-Vis, the PVP layer of the LSCs in which CDs are embedded tends to crack, as visible in **Figure 16(a), (c)** and **(d)**, probably due to exposure to heat or due to

aging. Due to the cracking, part of the PVP layer starts to peel off, partially decreasing the efficiency of the LSCs. To solve this problem, another type of LSC configuration was tested, with the PVP layer embedded in between two glasses to form a sandwich. This type of configuration resulted in being much more stable and resistant to aging.

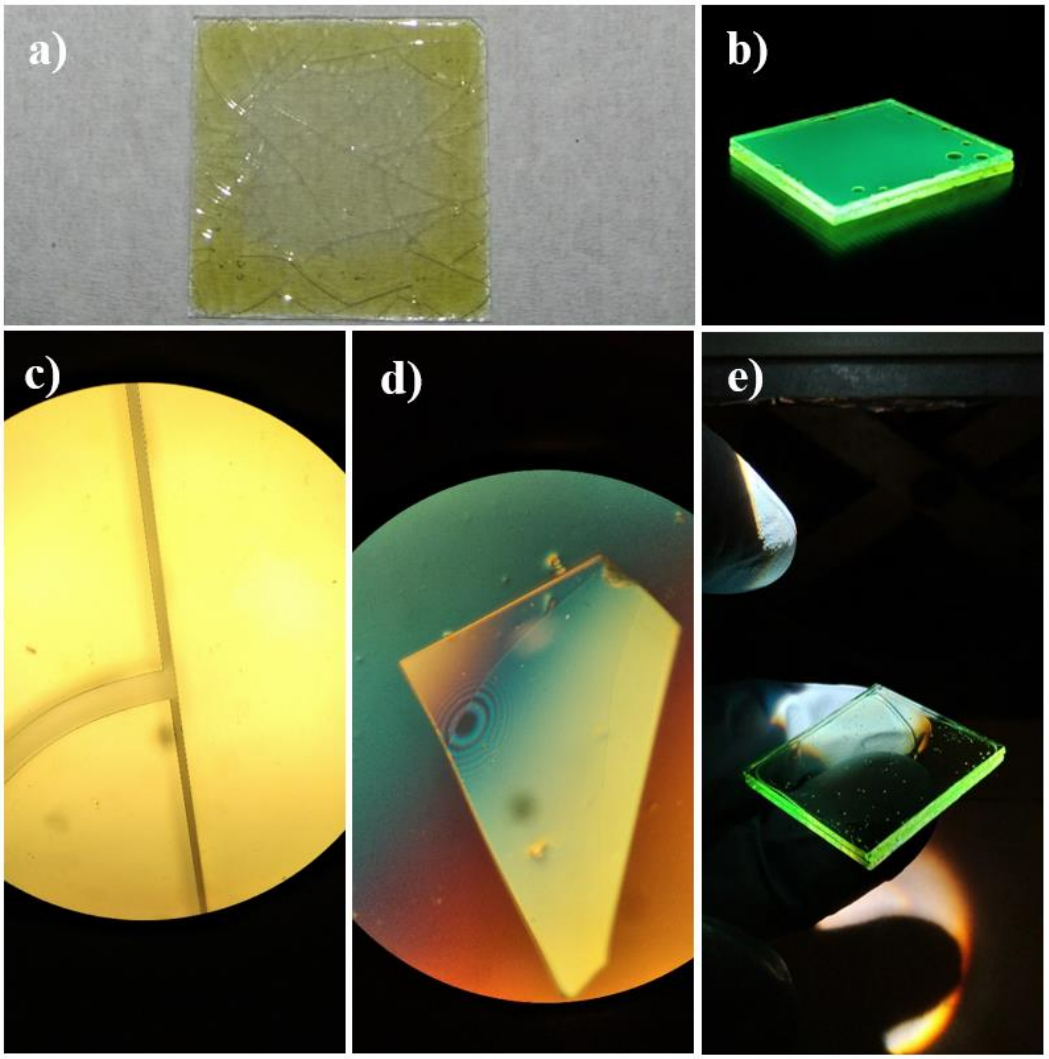

Figure 16 (a) *Single glass LSCs cracked after heat exposure,* ***(b)*** *sandwich LSCs under UV light,* ***(c)****cracks of the LSCs under optical microscope with transmitted light* ***(d)*** *fragment of LSCs under polarized light and* ***(e)*** *sandwich LSC under simulated solar light*

Figure 16 (b) and **(e)** show sandwich LSCs under UV irradiation (395 nm) and under solar simulator light. As visible in the pictures, the PVP of the sandwich structure did not break even after long exposures to heat and simulated solar light.

3.2.2 Uv-Vis characterization

The CDs LSCs analyzed with UV-Vis spectroscopy in range 300 to 700 nm show a single broad absorption peak at 406 ± 50 nm, while the absorption peak of the CDs in liquid sample (ethanol and PVP) is at 412 **Figure 17(a)**. In the case of the Uv-Vis of the CDs LSC, a second peak appears at 290 nm, and it is probably related to the PVP matrix. This second peak appears also in the absorption spectrum of the CDs dispersed in ethanol and PVP, which is reported in **Figure 17(c)**. In the same picture it is also reported the absorption spectrum of CDs dispersed in ethanol without PVP in which the peak at 290 nm is absent. The PVP mainly absorbs wavelengths shorter than 300 nm, with a maximum peak at 290 nm as reported in the literature [62]. Since the absorption peak of PVP is far from the absorption peak of CDs, the PVP can be considered a good matrix to embed the CDs in CDs LSCs because its absorption peak does not overlap with the absorption peak of the CDs. According to the Uv-Vis spectrum of the CDs LSCs **Figure 17(a**), most of the absorption of the CDs LSCs is in the UV, violet and part of indigo light, while absorption intensity becomes flat at values bigger than 450 nm. Therefore, the CDs LSCs have low absorption of visible light, which confirms that they are suitable for installation on windows, since they are highly transparent to visible light.

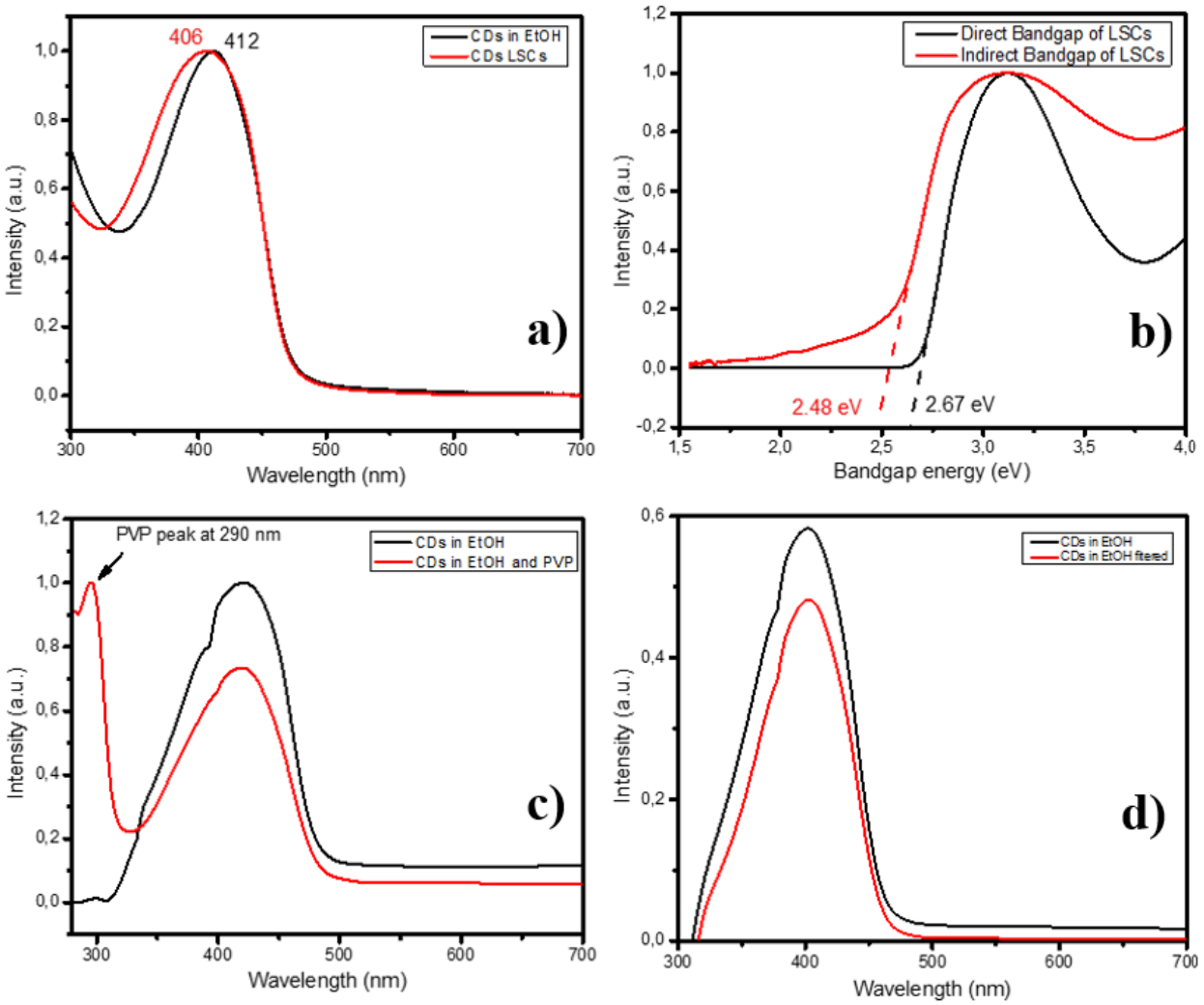

Figure 17 (a) *absorption spectra of CDs dispersed in ethanol and CDs LSCs,* ***(b)*** *direct and indirect bandgaps of CDs LSCs calculated from the absorption spectra using the Tauc plot,* ***(c)*** *absorption spectra of CDs in different liquid media,* ***(d)*** *comparison between absorption spectra of filtered and non-filtered CDs*

The absorption spectrum of CDs in ethanol was recorded before and after the filtration with a silica gel column and it is reported in **Figure 17(d)**. As visible from the figure, the filtration does not change the shape and the position of the absorption peak but it only affects the intensity of the peak, probably because during the filtration part of the CDs is lost. From the Uv-Vis spectrum of the CDs LSCs, it was also possible to estimate their optical direct and indirect band gap using the Tauc plot **Figure 17(b)**. The direct band gap results to be of 2.67 eV, which corresponds to the energy of a photon with a wavelength of 464 nm (blue region) while the indirect bandgap results in being of 2.48 eV, which corresponds to the energy of a photon with a

wavelength of 500 nm (cyan region). These results were compared to PL data to determine which of the two band gaps is the correct one. The PL emission peak was found to be at 530 nm and the energy of a photon with this wavelength is 2,34 eV, which is nearer to the energy of the calculated indirect band gap (2.48 eV) than the energy of the calculated direct bandgap (2.67 eV). Consequently, the LSCs are supposed to have an indirect band gap. Going back to the absorption peak of the LSCs centered at 412 nm, it is possible to predict which electronic transition is responsible for this absorption. In **Figure 18** are reported the positions of the absorption peaks of CDs that are expected in a UV-Vis spectrum[63]. According to the scheme, the electronic transition responsible for an absorption peak at 412 nm might be caused by the excitation of the core or the shell of the CDs, since this peak falls near the border between band B and band C.

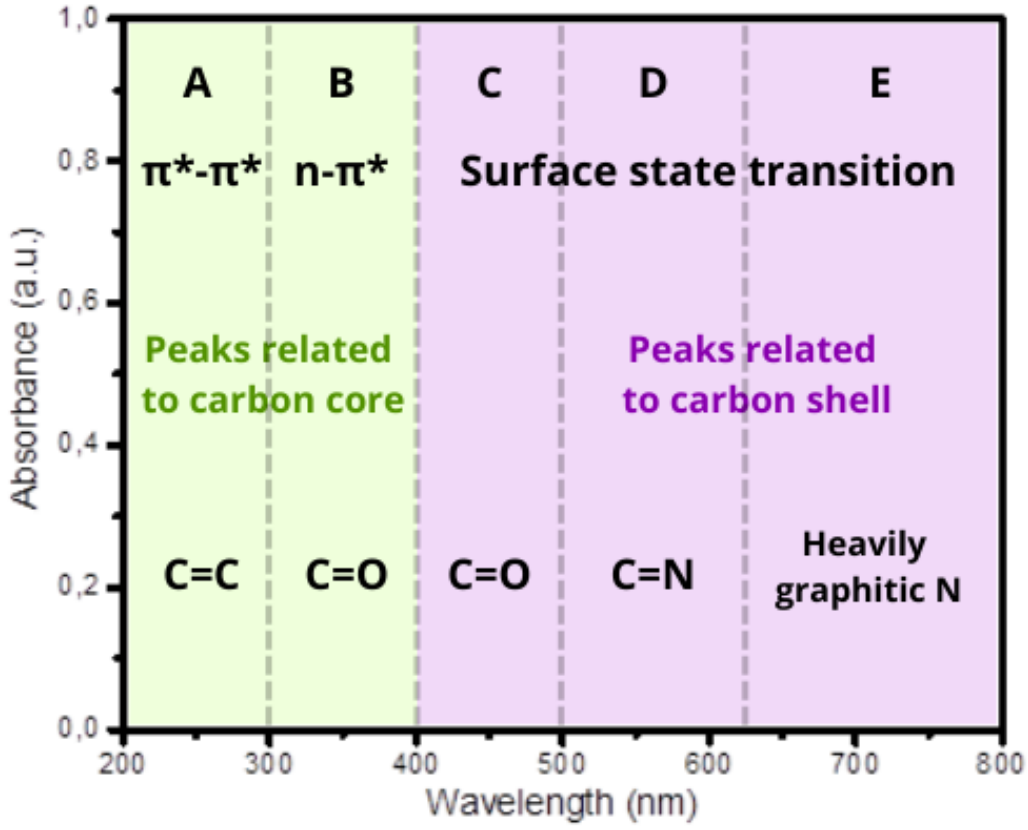

Figure 18 *A schematic illustration of the relationship between the absorption spectrum and electron transition of CDs*

In both cases is involved a transition of the C=O groups. An absorption peak similar to that at 412 nm of the LSCs was also reported in the literature[64].

3.2.3 PL characterization

3.2.3.1 PL mapping

To determine the peaks of maximum excitation and emission of the CDs, a PL mapping was performed exciting the liquid sample with CDs dispersed in ethanol and PVP. The sample was excited from 250 nm to 500 nm and the PL emission was recorded from 300 nm to 750 nm. All the intensities were normalized dividing them by the highest value of intensity, the mapping is reported in **Figure 19**. In the figure are visible two main emission peaks, one at excitation of 280 nm and emission at 514 nm and the second one at excitation of 395 nm and emission at 510 nm. The first peak is less intense than the second and its excitation wavelength (280 nm) is very near to the absorption wavelength of PVP that is 290 nm. Therefore, this emission peak might be caused by the presence of the PVP. The second peak is the most intense and its emission is in the cyan region (500-520 nm).

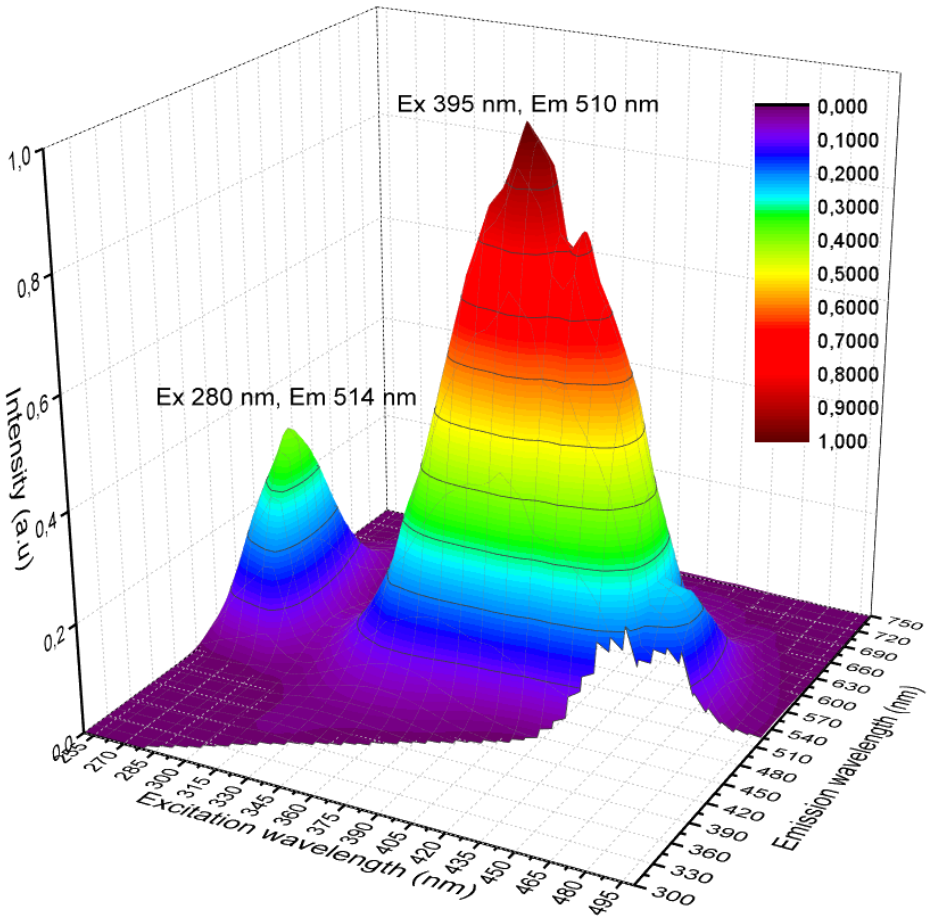

Figure 19 *Emission mapping of the CDs in ethanol/PVP solution*

The maximum excitation for the second peak is near to the absorption peak of CDs that was reported in the Uv-Vis characterization (406 nm), this suggests that this emission peak is related to the CDs. It is to notice that the excitation of both the two peaks in the emission mapping (280 and 395 nm) is shifted by 10 nm with respect to the corresponding absorption peaks of the Uv-vis analyses that were at 290 nm and 406 nm.

In **Figure 20(a)** it is reported the same CDs emission mapping of the previous figure but here all the emission curves were normalized individually to find the maximum emission peak of each curve. According to this mapping, under excitation in the range 250-475 nm the CDs emission does not change significantly, and it is at 510 ± 10 nm. This means that the emission of the CDs is not dependent on the wavelength of excitation. As it was written above, a wavelength of 510 nm corresponds to a photon of 2.43 eV, that is very near to the value of the indirect bandgap

(2.48 eV) of the LSCs that was calculated with the Tauc plot. This means that the Tauc plot is a reliable method to calculate the indirect band gap of the CDs from their Uv-Vis spectrum.

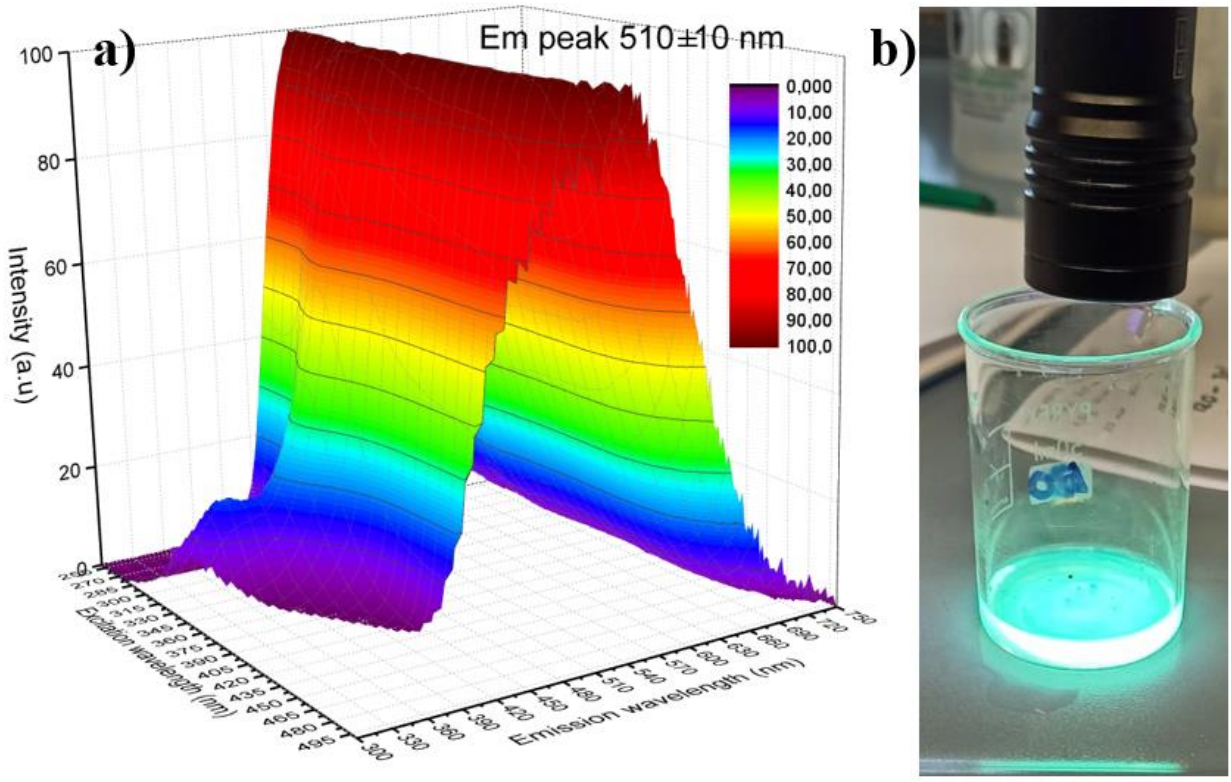

Figure 20 (a) *Emission mapping of the CDs normalized and* ***(b)*** *CDs under 395 nm light irradiation*

The emission at 510 nm corresponds to a photon in the cyan region and explains the cyan color of the CDs that can be observed when they are irradiated with the UV torch (395 nm) **Figure 20(b).** An explanation for the optical behavior of the CDs is that they absorb UV light at different wavelengths with a main peak at 406 nm, the absorption causes the electrons of the valence band to jump to the conduction band of the CDs. From the conduction band, the excited electrons disperse energy through non radiative relaxation and reach the bottom of the conduction band. From the bottom of the conduction band, electrons go back to the top of the valence band through radiative relaxation, which causes an emission of a photon with an energy equal to the energy of the bandgap (2.48 eV), which correspond to the cyan color that is visible in **Figure 20(b)**. A more detailed explanation of the optical behavior of the CDs and of the band theory will be discussed in the chapter on TRPL characterization. An emission mapping was performed on the LSC to compare it with the emission mapping of CDs in liquid sample and

detect any change in emission peaks. The mission mapping of CDs in ethanol/PVP and the emission mapping of the CDs LSC are reported in 2D in **Figure 21(a)** and **Figure 21(b).** The two samples show two main peaks in similar positions (the mapping of CDs in ethanol/PVP was described above).

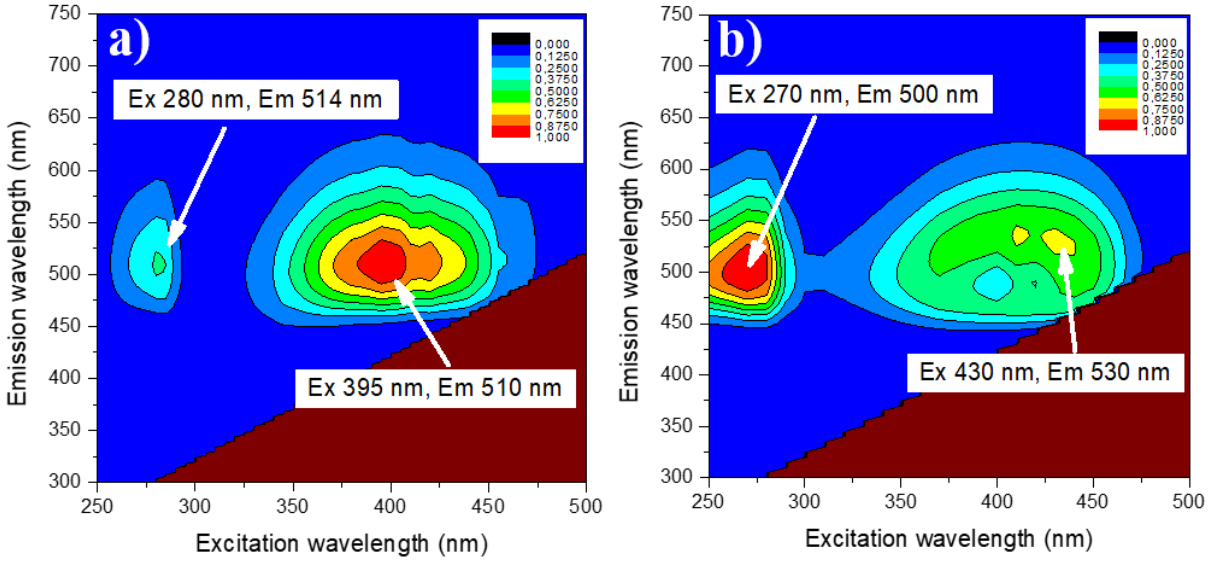

Figure 21 *2D representation of emission mapping of* ***(a)*** *CDs dispersed in ethanol/PVP and* ***(b)*** *CDs LSC*

In the case of the LSC mapping, the two emission peaks appear at 500 and 530 nm. The peak at 530 nm has a maximum excitation at 430 nm while the corresponding peak in case of liquid sample was at Ex=395 nm and Em=510 nm). This means that both emission and excitation of the peak in case of the LSC are redshifted if compared with those of the liquid sample. The other peak that has an excitation of 280 nm and an emission of 514 nm in the liquid sample, in the LSC is visible at an excitation of 270 nm and emission of 500 nm. In this case, the peak in LSCs mapping appears blue shifted if compared to the same peak in the liquid sample. It is to notice that the emission peak of the PVP (Ex 280 nm) in the mapping of the liquid sample is less intense than the peak related to CDs (Ex 395 nm) while it is the opposite in the LSC mapping. The LSC differs from the liquid sample for the presence of the glass substrate, for a lower concentration of CDs and for the state of the PVP that is liquid in the case of the CDs and solid in the case of the LSC. Due to a lower concentration of CDs in the LSC with respect to the liquid sample, the emission peak of CDs is lower than that of PVP. On the other hand, in the liquid

sample the peak of CDs emission is higher than that of PVP because in liquid sample the CDs are highly concentrated.

3.2.3.2 PL spectrum

A PLE spectrum of the LSC was recorded with the emission fixed at 530 nm, which is the wavelength of maximum emission according to the PL mapping. The aim of the PL spectrum is to find the best excitation wavelength for the LSC with precision and to detect if there is any other excitation peak that was not visible in the PL mapping. The PLE spectrum of the LSC reported in **Figure 22** shows two excitation peaks at 276 and 416 nm, the second one with a higher intensity than the first one.

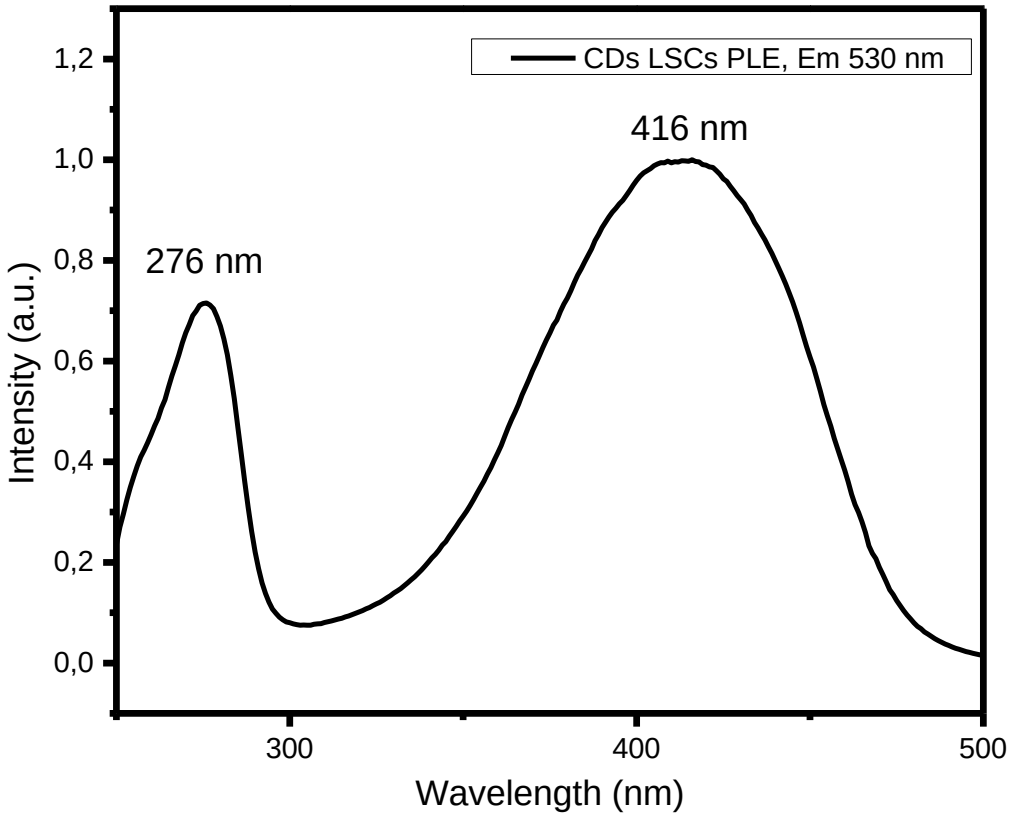

Figure 22 *PLE of the LSCs with emission fixed at 530 nm*

3.2.4 Stokes shift

From the UV-Vis and from the PL emission spectra of the LSCs it was possible to calculate their Stokes shift, which is reported in **Figure 23**. The LSCs result in having a Stokes shift of 0.71 eV, which is not big enough to separate the absorption and the PL emission peaks of the CDs. Consequently, part of the photons emitted by a CD might be reabsorbed by other CDs as they are travelling through the LSC. This means that part of PL photons will not reach the LSC edges, where the PV cell is placed to produce energy. Photon reabsorption phenomena can negatively influence the efficiency of the LSC, and this is why in LSC a wide Stokes shift is normally preferred instead of a narrow one. On the other hand, the side effect of having a large Stokes shift is that a lot of the solar energy that is collected by the LSC is lost into non-radiative emission.

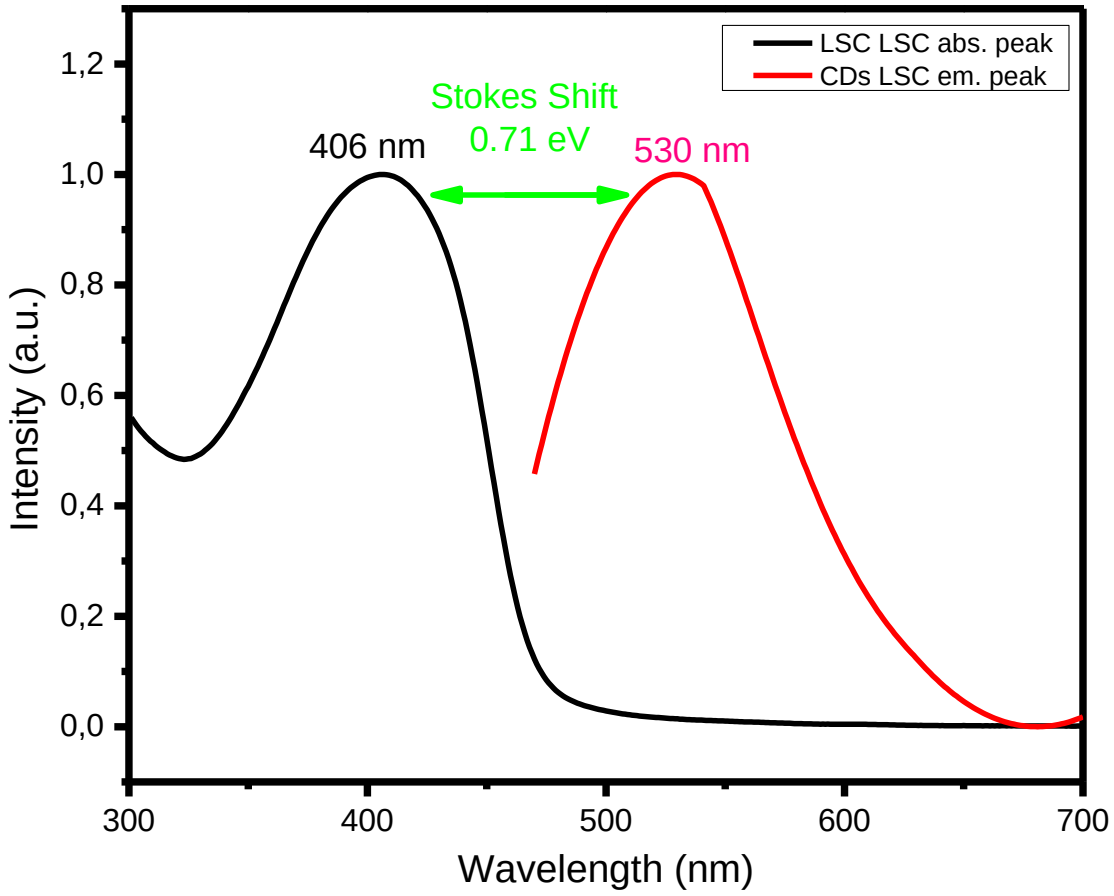

Figure 23 *representation of the Stokes shift of the LSCs*

The best way to avoid photon reabsorption in LSC while at the same time limit non-radiative relaxation phenomena would be to select fluorophores that have very narrow absorption and PL emission peaks, such that these two peaks do not overlap. On the other hand, a fluorophore with narrow absorption cannot exploit the solar spectrum efficiently and this can decrease the QY. To have a high QY is therefore necessary to find the right balance between shape, position and width of absorption and PL emission peaks of the fluorophore embedded in the LSC.

3.2.5 Quantum Yield

The QY of the LSCs was measured under an excitation of 405 nm, which is a value near to the absorption peak of the LSCs. The QY results to be of 60.8 %, which is very promising considering that the synthesis process of the CDs might be optimized with further studies. Moreover, the QY of the CDs in the liquid sample was found to be even higher than the one of the LSC, in fact it resulted in being 75.9% for the CDs dispersed in ethanol/PVP. Therefore, when used in LSCs, the QY of the CDs is reduced by about 20%. The explanation for these decreases might be related to the photon reabsorption phenomena caused by the narrow Stokes shift that were described above. Another reason for the loss in QY might be related to the difference in CDs concentration between the liquid sample and the LSCs. Moreover, it must be considered that after the CDs are drop-cast on the glass substrate, their concentration changes because part of the ethanol in which they are dispersed evaporates. The QY of the LSCs might be also influenced by non-uniform coverage of the glass substrate with the CDs layer and by the cracks of the PVP matrix. The QY of the LSC was measured a second time after the cracking of the PVP and it resulted in decreasing from 60.8% to 59.4%.

3.2.6 Time resolved photoluminescence analyses

The last optical characterization performed on the LSCs is the TRPL. The time decay of the excited electrons was measured under an excitation of a 372 nm pulsed laser at three different emission wavelengths that are 450, 500 and 510 nm. The TRPL results are reported in **Figure 24**. The TRPL measured at 450 nm PL emission showed two different populations of time decays of respectively 4.05 ns and 12.84 ns. The time decay of 12.84 ns is like time decays that were later observed in TRPL measured at 500 and 510 nm, so they are supposed to be generated by the

same transition. On the other hand, the time decay at 4.05 only appears in the TRPL at 450 nm PL emission. This short time decay is probably related to an electron transition different from that of 12.84 ns and it might be related to the PVP or to the presence of small CDs with very few carbon atoms. A CDs with few carbon atoms are expected to have a narrow conduction band, therefore, the non-radiative relaxation of the excited electrons will be faster than the relaxation that occurs in bigger CDs. In the case of 500 nm and 510 nm emission, the LSC shows a single population of time decay of excited electrons that corresponds to 14.8 ns in the case of PL emission at 500 nm and 15.37 ns in the case of PL emission at 510 nm. It is to remember that a photon of 500 nm has a corresponding energy of 2.48 eV while a photon of 510 nm has an energy of 2.43 eV to justify these values using band theory that will be discussed.

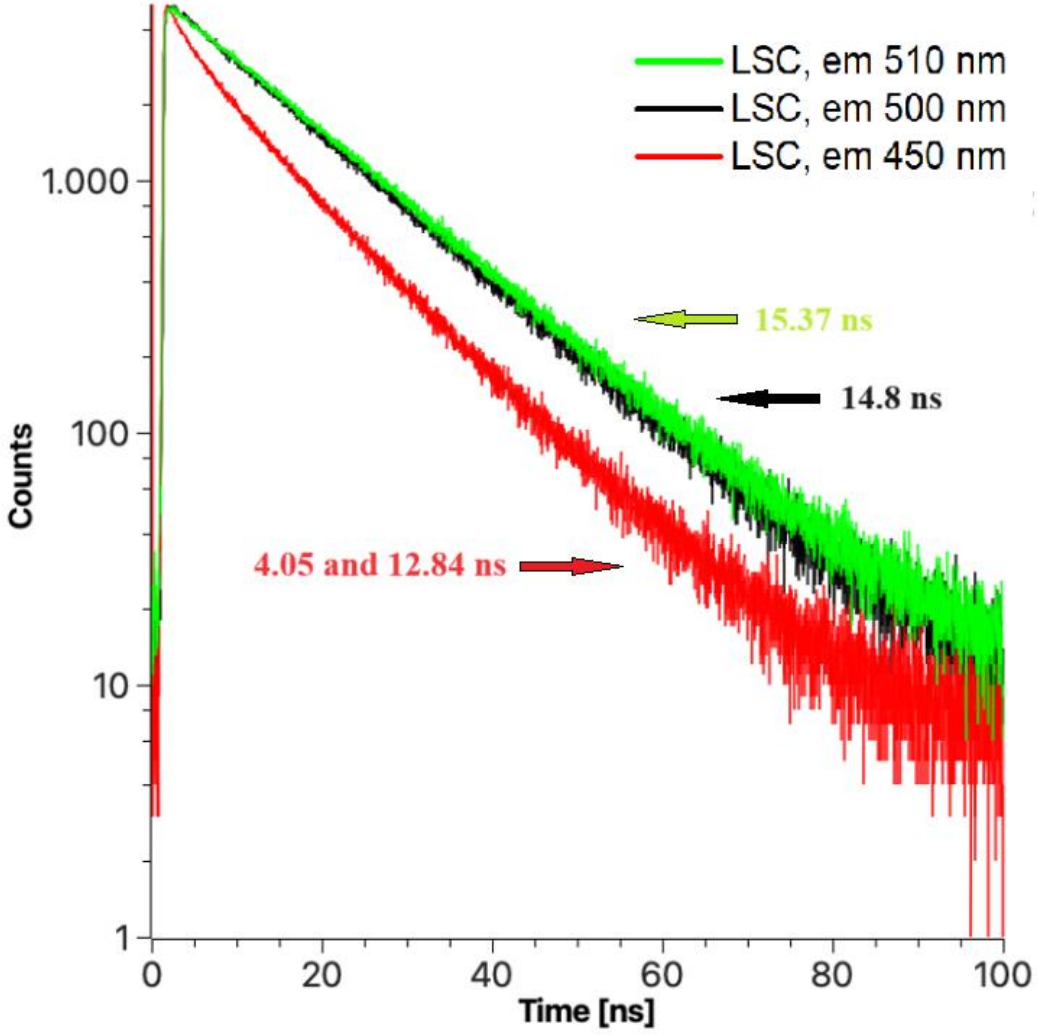

Figure 24 *TRPL of the CDs LSC under 372 nm excitation and PL emissions at 450, 500 and 510 nm*

For a better explanation of the band theory, a sketch of the band structure of the synthesized CDs is reported in **Figure 25**. It can be imagined that under irradiation with a 372 nm pulsed laser, an electron of the CDs is excited from the valence to the conduction band (violet arrow in the sketch). This electron will then relax non-radiatively (red arrows) to reach the bottom of the conduction band of the CDs. In a conduction band, the energy levels with lower energy are disposed at the bottom of the band. Therefore, the energy level of 2.43 eV (that corresponds to a photon of 510 nm) is nearer to the bottom of the conduction band with respect to the energy level of 2.48 eV (that corresponds to a photon of 500 nm). This means that an excited electron during its non-radiative relaxation process will take more time to reach the energy level of 2.43 eV than an energy level of 2.48 eV.

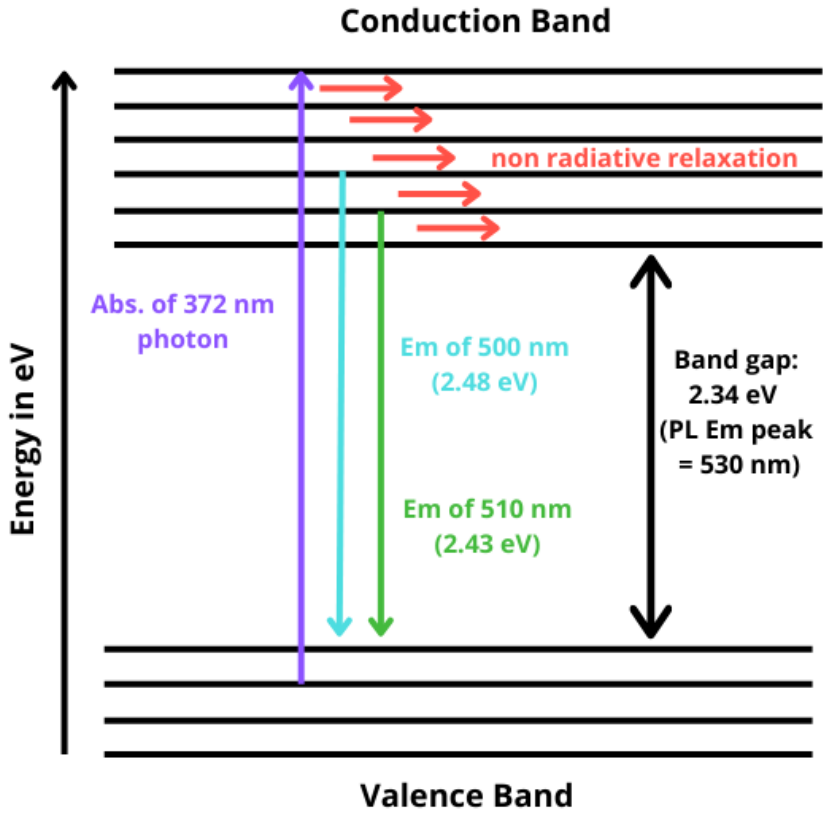

Figure 25 *schematic representation of the optical features of CDs LSCs including band gap, photon absorption, non-radiative electron relaxation and PL emission. For the band gap it was used the energy corresponding to the wavelength of maximum PL emission (530 nm)*

Once an electron has reached an energy level, it can jump directly from it to the top of the valence band, emitting a photon with the same energy of the gap between the two levels. This

means that electrons that are in the energy level of 2.43 eV of the conduction band can jump to the top of the valence band emitting a photon of 510 nm (green arrow). The time decay of these electrons will be slower than the time decay of electrons jumping to the top of the valence band from an energy level of 2.48 eV.

Summary of optical characterization

	Abs peak	**Em peak**	**Stokes shift**	**QY (ex 405 nm)**
For CDs in EtOH/PVP				60.80%
position in nm	406	530	--	
energy in eV	3.05	2.34	0.71	
For CDs LSCs				75.90%
position in nm	412	510	--	
energy in eV	3.01	2.43	0.58	

Summary of TRPL results

TRPL of CDs LSCs Ex 372 nm	**τ1 [ns]**	**τ2 [ns]**	**β1 [counts]**	**β2 [counts]**
Em 450 nm	4.05	12.84	1591	3268
Em 500 nm	--	14.8	--	4865
Em 510 nm	--	15.37	--	4857

3.3 Current-Voltage measurements

In Figure 26 (a-e) are reported the I-V curves that were measured on the PV cell coupled with the LSCs. All the LSCs analyzed differ among each other for CDs concentration, thickness of the CDs/PVP layer, purity of the CDs and structure of the LSC. The black line in **Figure 26(a)** is the I-V curve measured on the PV cell without coupling it with any LSC and it can be considered as a blank. The PV cell during this measurement was not directly irradiated by the solar simulator, anyway, a small amount of light was reflected by the walls of the black box, and it was able to reach the cell surface. That is why the PV cell was still able to produce a small current even if not directly irradiated by the solar simulator. In the same figure it is shown the I-V curve of a simple glass (red line) that is the substrate used in all LSCs, as expected the current produced by the PV cell coupled with the glass is higher than the one of the blank because some of the light

collected by the glass is converged on its edges, where the PV cell is placed. These two I-V curves (PV cell and Glass) will be shown in all graphs as reference curves. Still in **Figure 26(a)** there is the first comparison between the I-V curves of two LSCs. Both LSCs were prepared with a CDs solution/PVP ratio of 1:3. The first LSC (violet line) was produced with 0.5 ml of CDs/PVP mix while the second one (yellow line) was produced with 1 ml of the mix. Both curves indicate an increase in the intensity of the current produced by the PV cell with respect to the two references. On the other hand, the two curves do not differ significantly in position, which means that increasing the amount of the CDs/PVP mix from 0.5 ml to 1 ml does not increase LSC efficiency. This is probably why an amount of 0.5 ml of CDs/PVP mix on a 2.5 x 2.5 glass substrate is sufficient to absorb all the photons provided by the solar simulator at this light intensity. In **Figure 26(b)**, the I-V curves for the non-filtered and filtered CDs LSC are compared. The two LSCs have the same CDs concentration and the same amount of CDs/PVP mix (0.5 ml). The filtration of CDs with the silica column improved the efficiency of the LSC, in fact, the I-V curve of the LSC with filtered CDs (blue line) has higher values than the LSC with non-filtered CDs (violet line). Filtration probably removes synthesis byproducts and part of the bigger CDs, reducing the scattering of the photons that travel through the LSC. Scattering phenomena can significantly reduce the guideline efficiency of the LSC because they decrease its transparency. In fact, after filtration the solution of CDs and ethanol resulted in being less turbid. Moreover, the filtered CDs demonstrated to be more stable than the non-filtered ones. While the non-filtered CDs dispersed in ethanol tend to partially sediment after few days, the sedimentation of filtered CDs was not observed even after few months. Filtration also decreases the concentration of CDs in the solution because part of them remains blocked in the filtering column. This means that the improvement of the I-V curve due to CDs filtration might also be caused by the dilution of the CDs. In fact, a too high CDs concentration in the LSC can cause the photon reabsorption phenomena that were described in the chapter on Stokes shift

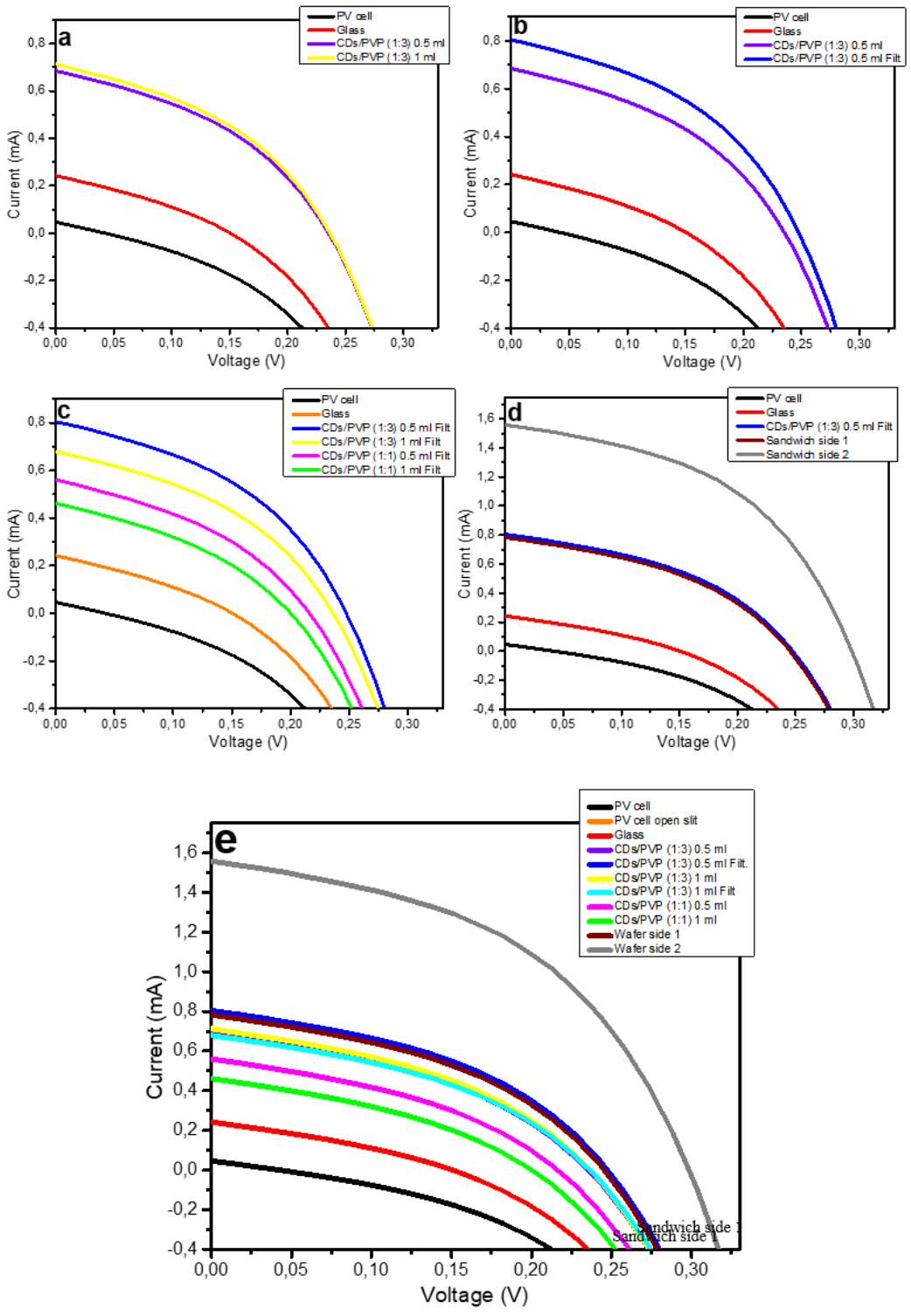

Figure 26 (a) *I-V curves of LSCs with different CDs-PVP amount,* ***(b)*** *LSCs with filtered and non-filtered CDs,* ***(c)*** *LSCs with different amounts of CDs,* ***(d)*** *single glass and double glass (sandwich) LSCs,* ***(e)*** *all the LSCs compared*

To better determine the effect of CDs concentration and the effect of the thickness of the CDs/PVP layer on the LSC efficiency, it was measured the I-V curve of LSCs with different CDs/PVP ratios and with different amounts of CDs/PVP mix. All these samples were prepared using CDs of the same batch to make their I-V curves comparable. The results are reported in **Figure 26(c).** The efficiency of the LSCs decreases when passing from a CDs/PVP ratio of 1:3 to a ratio of 1:1 and passing from 0.5 ml to 1 ml. This means the right CDs concentration for the best LSCs efficiency is probably at a CDs/PVP ratio ≤ 1:3 and that the right amount of CDs/PVP mix is ≤ 0.5 ml. However, it would be difficult to cover a 2.5 x 2.5 cm glass substrate with less than 0.5 ml of mix using the drop-casting deposition, consequently, other type of depositions must be tested such as spin-coating and doctor blade coating. Moreover, these last two methods should also guarantee a more homogeneous thickness of the CDs/PVP layer, which can improve the guideline efficiency of the LSCs. Finally, in **Figure 26(d)** the best I-V curve of all the already discussed ones (that is the one of the LSC with 0.5 ml of filtered CDs/PVP (1:3) (blue line)), is compared with the I-V curve of the sandwich LSCs that was prepared with 0.7 ml of non-filtered CDs/PVP (1:3) (brown line, "Sandwich side 1"). In the sandwich LSC it was used an amount of CDs/PVP mix of 0.7 ml instead of 0.5 ml because part of the solution is lost during the fabrication of the sandwich. As visible in the figure, the two curves overlap almost perfectly. This means that the sandwich structure does not affect the efficiency of the LSC, while it has the advantage that it protects the PVP from cracking and aging. An interesting result was obtained flipping the sandwich upside down and measuring its I-V curve again (grey line, "Sandwich side 2"). In this case, the I-V curve results in being much higher than the one measured on the same sandwich LSC, and consequently it is also higher than all the other I-V curves measured on all the other LSCs, as reported in **Figure 26(e)**. An explanation for the high efficiency of the upside-down sandwich might be related to a mismatch between the alignment of the two glasses of the sandwich LSC, which is caused by a small difference in their size **Figure 27 (a)** and **(b).** The size difference between the glass at top and the glass at the bottom of the LSC is intentionally exaggerated in the sketches for an easier understanding of the phenomenon, the actual difference is less than 1 mm.

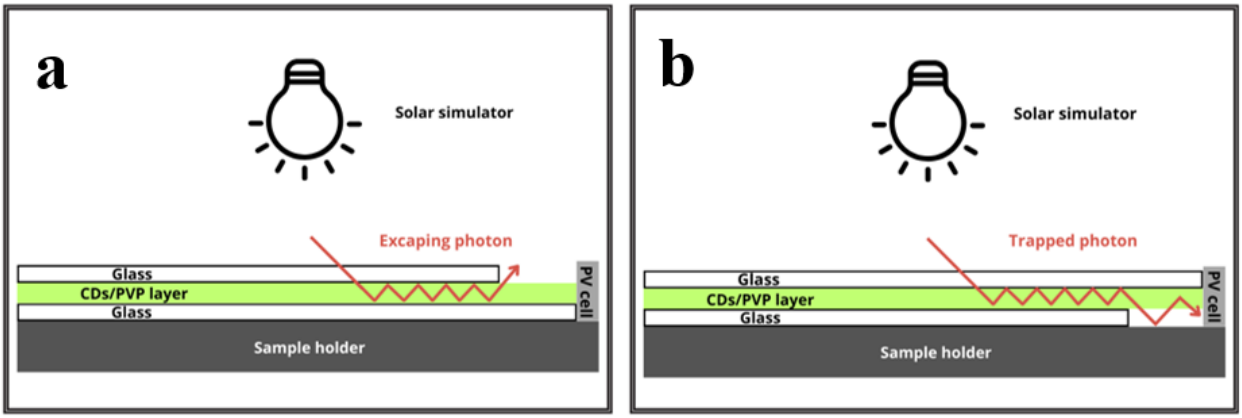

Figure 27 (a) *sandwich LSC with bottom glass longer than the upper glass and* ***(b)*** *sandwich LSC flipped upside down. The sketches are not in scale*

In the first case **Figure 27(a)**, the upper glass is shorter than the bottom one, therefore, part of the photons that are guided toward the edges of the LSC escape before reaching the PV cell. When the LSC is flipped upside down, the upper glass blocks photons from escaping the LSC, so the intensity of the irradiation at the surface of the PV cell will be higher than the one in the first case and the intensity of the current produced by the PV cell will be higher.

4. Conclusions

Eco-friendly carbon dots fluorophores were synthesized through a cheap and simple method and were successfully employed to produce high-efficiency LSCs. The size of CDs turned out to be non-uniform and presented two different size populations of respectively 13 ± 2 and 22 ± 2 nm, which means that the proposed synthesis method does not allow to tune CDs size. However, further experiments might lead to a better understanding of the formation and growing process of the CDs, allowing better control of particle size and size distribution. A possible strategy to investigate CDs formation and growth processes might consist in analyzing with HRTEM small quantities of CDs withdrawn at different steps of their synthesis. In this way it would be possible to monitor the changes that the CDs undergo during their synthesis. It is important to have better control on CDs size because it can affect both position and width of their emission peak. It is to remember that the position of the emission peak influences the Stokes shift and QY, which are both important to optimize LSCs efficiency. The XRD measurements suggest that the core of CDs has the crystal structure of graphene, while, according to the IR spectrum, the shell of the

CDs presents different functional groups among which O-H, C=O, C-O-C and N-H groups. According to UV-Vis analyses, LSCs have two main absorption peaks at 290 nm (related to PVP) and at 406 nm related to transitions of the C=O bonds present in the carbon core or in the carbon shell. Since the absorption peak of PVP and that of CDs are far from each other, they do not interfere, which confirms that from an optical point of view the PVP is a good matrix to embed the CDs in LSCs. The UV-Vis spectrum of the CDs embedded in the LSCs confirmed a broad absorption of UV light and low absorption of visible light, which allows them to efficiently exploit big part of the UV light of the solar spectrum to produce energy while they remain transparent to the visible part, which is very important for LSCs applications on windows. The indirect bandgap of the LSCs calculated with the Tauc plot from the UV-Vis spectrum resulted to be of 2.48 eV, which corresponds to the energy of a photon of 500 nm, which is in accordance with the emission peak of the CDs in liquid solution that is centered at 510 nm. The CDs dispersed in ethanol and PVP resulted in having two emission peaks, one that is probably related to the PVP (ex 280, em 514 nm) and one at that is more intense than the first one and that is related to the CDs (ex 395, em 510 nm). The LSCs result in having the same emission peaks of CDs in ethanol/PVP but slightly shifted: one at ex 270 and em 500 nm for the PVP and one at ex 430, em 530 nm for the CDs. In the case of the LSCs, the first peak is more intense than the second. The differences in peak intensities between the CDs in liquid and the LSCs are probably related to the different concentrations of the CDs in the two samples. The LSCs result in having a Stokes shift of 0.71 eV that is not high enough to separate their absorption and emission peaks. The overlap of the two peaks can cause photon reabsorption phenomena that can decrease the efficiency of the LSCs. Some strategies to decrease photon reabsorption are the broadening of the LSCs Stokes shift or the narrowing of their emission peak. In any case, to obtain these changes it would probably require modifications of the CDs synthesis process. The QY of the CDs dispersed in ethanol and PVP resulted in being 75.9% under an excitation of 405 nm. This is a very encouraging result, considering that it was recorded on non-filtered CDs and that filtration might even increase the QY of the CDs. On the other hand, the QY of the LSCs is 60.8%, which means that it is reduced by 20% with respect to the one of the CDs in liquid. This loss in QY can be caused by the cracks that form on the PVP during aging or exposure to heat or by a non-optimized CDs concentration in the LSCs. The thickness and the irregularity of the PVP/CDs layer might also be responsible for the loss in QY, a thinner and

more uniform deposition of the layer can be reached by spin coating. According to TRPL measurements, the LSCs present a single time decay of 15.37 ns when the measurement is performed under 372 nm of excitation and at an emission of 510 nm. The I-V curve measurement evidenced that, of all the fabricated LSCs, the best efficiency is obtained with a CDs/PVP ratio of 1:3 and an amount of CDs/PVP of 0.5 ml and that the LSCs with filtered CDs have better I-V curves than the LSCs with non-filtered CDs. Filtration also makes the CDs much more stable when dispersed in ethanol, preventing them from precipitating. Finally, the best I-V curve was obtained with a LSC with a sandwich structure. This means that the sandwich structure of the LSCs not only protects the PVP from heat exposure and aging, but also improves the guideline efficiency of the LSCs. The black box that was designed, 3D printed and used as a connector resulted to be fundamental for the recording of reliable data during I-V curve measurements. In fact, it allowed to perform all measurements at the same conditions for every LSC, standardizing the procedure for these measurements. To conclude, some suggestions will be proposed to increase the QY and the efficiency of the produced CDs LSCs; the concentration of CDs in the LSCs must be optimized to avoid saturation. To do so, it is important to determine the actual concentration of CDs after their synthesis. Such information might be obtained with a dynamic light scattering spectroscopy, which also gives information on the size distribution of the particles. The PVP matrix can be substituted with another polymer that does not cracks with aging and heating, which significantly decreased the QY of the LSCs with respect to that of CDs in ethanol.

5. Acknowledgments

First, I want to thank Professor Kassa Belay Ibrahim, during this internship he has demonstrated constant patience and given immeasurable encouragement to develop my ideas further.

I want to thank Professors Elisa Moretti and Alberto Vomiero for accepting me into the group "Nano4GEA" for this internship and for always being a point of reference. I also want to thank Professor Moretti for her contagious enthusiasm for teaching chemistry, it pushed me to deepen my knowledge of nanomaterials for green energy applications.

Thanks to Alessandro Boscolo Palo, whose help with the black box project was fundamental to this thesis. Thanks to Professor Shujie You for training me and sharing her extensive knowledge during my Erasmus experience at the Luleå Technology University. Thanks also to all the new friends that I met and adventured with during my Erasmus time in the Swedish Lapland.

Thanks to all the people of "Beta lab" for sharing their culture, stories and food with me. I want to thank Mahnoor Hassan for her help during my internship, Muzammil and Dr. Pratik for their good company, laughs and many interesting conversations that we had in the laboratory. Thanks to Dr. Darshan for his interest in both my work and ideas, and for his precious suggestions. Thanks to everyone at "Eta lab" and all the members of the group Nano4GEA that were always ready to help. Thanks to Sara and Francesca, the two very committed Bachelor students that patiently listened to all my explanations and worked hard by my side during the last months with endless interest. Thanks to Professor Enrico Trave for sharing his knowledge and for always being available for any explanation.

Thanks to all the fellow students of the master's degree in science and technology of Bio and Nanomaterials, who share the same interest and enthusiasm for the nano world and thanks to all the friends who demonstrated their curiosity about what I am studying.

Finally, I want to conclude with a special thanks to my family for their continuous support given to me during my time at university.

6. References

1. O'Sullivan JN. Demographic Delusions: World Population Growth Is Exceeding Most Projections and Jeopardising Scenarios for Sustainable Futures. *World*. 2023;4(3):545-568. doi:10.3390/world4030034

2. Gu D, Andreev K, Dupre ME. Major Trends in Population Growth Around the World. 3(28).

3. Taagepera R, Nemčok M. World population growth over millennia: Ancient and present phases with a temporary halt in-between. *Anthr Rev*. 2024;11(1):163-183. doi:10.1177/20530196231172423

4. Mattick CS, Williams E, Allenby BR. Energy and civilization: A history of energy production and consumption in a global cultural, technological and economic context. In: *2009 IEEE International Symposium on Sustainable Systems and Technology*. IEEE; 2009:1-6. doi:10.1109/ISSST.2009.5156766

5. Martins F, Felgueiras C, Smitkova M, Caetano N. Analysis of Fossil Fuel Energy Consumption and Environmental Impacts in European Countries. *Energies*. 2019;12(6):964. doi:10.3390/en12060964

6. Kundu SN, Nawaz M, eds. *Sustainable Energy and Environment: An Earth System Approach*. Apple Academic Press; 2020.

7. Mikhaylov A, Moiseev N, Aleshin K, Burkhardt T. Global climate change and greenhouse effect. *Entrep Sustain Issues*. 2020;7(4):2897-2913. doi:10.9770/jesi.2020.7.4(21)

8. Earth's CO2 Home Page. Accessed April 27, 2024. https://www.co2.earth/

9. Global Monitoring Laboratory - Carbon Cycle Greenhouse Gases. Accessed April 29, 2024. https://gml.noaa.gov/ccgg/trends/

10. BloombergNEF. Accessed April 27, 2024. https://about.bnef.com/

11. Muhammad Abdul Basit, Saad Dilshad, Rabiah Badar, Syed Muhammad Sami ur Rehman. Limitations, challenges, and solution approaches in grid-connected renewable energy systems. doi:10.1002/er.5033

12. Bernd Zolitschka,Karl-Ernst Behre , Jürgen Schneider. Human and climatic impact on the environment as derived from colluvial, fluvial and lacustrine archives—examples from the Bronze Age to the Migration period, Germany. doi:https://doi.org/10.1016/S0277-3791(02)00182-8

13. Shereif H. Mahmoud, Thian Y. Gan. Impact of anthropogenic climate change and human activities on environment and ecosystem services in arid regions. doi:https://doi.org/10.1016/j.scitotenv.2018.03.290

14. M. Diesendorf a, T. Wiedmann. Implications of Trends in Energy Return on Energy Invested (EROI) for Transitioning to Renewable Electricity. doi:https://doi.org/10.1016/j.ecolecon.2020.106726

15. Khagendra P. Bhandari b, Jennifer M. Collier a, Randy J. Ellingson b, Defne S. Apul. Energy payback time (EPBT) and energy return on energy invested (EROI) of solar photovoltaic systems: A systematic review and meta-analysis. doi:https://doi.org/10.1016/j.rser.2015.02.057

16. Vladimir S. Arutyunov1,2 and Georgiy V. Lisichkin. Energy resources of the 21st century: problems and forecasts. Can renewable energy sources replace fossil fuels†. doi:10.1070/RCR4723

17. Axel Kleidon. Physical limits of wind energy within the atmosphere and its use as renewable energy: From the theoretical basis to practical implications. doi:https://doi.org/10.48550/arXiv.2010.00982

18. Sheikh Adil Edrisi, P.C. Abhilash. Exploring marginal and degraded lands for biomass and bioenergy production: An Indian scenario. doi:https://doi.org/10.1016/j.rser.2015.10.050

19. L’astronave Terra a corto di energia? | Areaperta. Accessed June 15, 2024. https://areaperta.pi.cnr.it/lastronave-terra-a-corto-di-energia/

20. A brief history of hydropower. Accessed April 29, 2024. https://www.hydropower.org/iha/discover-history-of-hydropower

21. History of Solar PV. Accessed April 29, 2024. https://www.renewableenergyhub.co.uk/main/solar-panels/history-of-solar-pv

22. Kim JY, Lee JW, Jung HS, Shin H, Park NG. High-Efficiency Perovskite Solar Cells. *Chem Rev*. 2020;120(15):7867-7918. doi:10.1021/acs.chemrev.0c00107

23. Yidan An, Nan Zhang, Zixin Zeng, Yating Cai, Wenlin Jiang, Feng Qi, Lingyi Ke,Francis R. Lin, Sai-Wing Tsang, Tingting Shi, Alex K.-Y. Jen, and Hin-Lap Yip. Optimizing Crystallization in Wide-Bandgap Mixed HalidePerovskites for High-Efficiency Solar Cells.

24. Alina Zaharia 1, , Maria Claudia Diaconeasa 1, , Laura Brad 2, , Georgiana-Raluca Lădaru 1,* and, Corina Ioanăs. Factors Influencing Energy Consumption in the Context of Sustainable Development. doi:doi:10.3390/su11154147

25. Rory V. Jones a, Alba Fuertes a, Kevin J. Lomas b. The socio-economic, dwelling and appliance related factors affecting electricity consumption in domestic buildings. doi:https://doi.org/10.1016/j.rser.2014.11.084

26. How Much Energy Does A Solar Panel Produce? | EnergySage. Accessed April 29, 2024. https://www.energysage.com/solar/solar-panel-output/

27. How much energy do solar panels produce for your home | YES Energy Solutions. Accessed April 29, 2024. https://www.yesenergysolutions.co.uk/advice/how-much-energy-solar-panels-produce-home

28. How much energy does a solar panel produce? Accessed April 29, 2024. https://www.solarreviews.com/blog/how-much-electricity-does-a-solar-panel-produce

29. Electricity consumption per capita by country 2022 | Statista. Accessed April 29, 2024. https://www.statista.com/statistics/383633/worldwide-consumption-of-electricity-by-country/

30. Electric power consumption (kWh per capita) | Data. Accessed April 29, 2024. https://data.worldbank.org/indicator/EG.USE.ELEC.KH.PC

31. Burcu Ozcan a, Ilhan Ozturk b. A new approach to energy consumption per capita stationarity: Evidence from OECD countries. doi:https://doi.org/10.1016/j.rser.2016.06.095

32. Bhuwan Pratap Singh a, Sunil Kumar Goyal a, Prakash Kumar. Solar PV cell materials and technologies: Analyzing the recent developments. doi:https://doi.org/10.1016/j.matpr.2021.01.003

33. Fuwen Zhao, Jixiang Zho, Dan He, Chunru Wang, Yuze Lin. Low-cost materials for organic solar cells. doi:DOI https://doi.org/10.1039/D1TC04097A

34. Stephen R. Forrest. The Limits to Organic Photovoltaic Cell Efficiency. doi:https://doi.org/10.1557/mrs2005.5

35. Leiping Duan, Ashraf Uddin. Progress in Stability of Organic Solar Cells.

36. Figure 1.1: Luminescent solar concentrators (LSC) are semi-transparent... ResearchGate. Accessed June 15, 2024. https://www.researchgate.net/figure/Luminescent-solar-concentrators-LSC-are-semi-transparent-plates-doped-or-coated-with_fig1_279824906

37. Review of the Fundamental Principles and Performances on Lminescent Solar Concentrators. Accessed April 29, 2024. https://www.e-asct.org/journal/view.html?doi=10.5757/ASCT.2021.30.1.14

38. Fluorescence - Wikipedia. Accessed April 29, 2024. https://en.wikipedia.org/wiki/Fluorescence

39. Diniz ASAC, Duarte TP, Costa SAC, Braga DS, Santana VC, Kazmerski LL. Soiling Spectral and Module Temperature Effects: Comparisons of Competing Operating Parameters for Four Commercial PV Module Technologies. *Energies*. 2022;15(15):5415. doi:10.3390/en15155415

40. Chander S, Purohit A, Nehra A, Nehra SP, Dhaka MS. A Study on Spectral Response and External Quantum Efficiency of Mono-Crystalline Silicon Solar Cell. Published online 2015.

41. Field H. Solar cell spectral response measurement errors related to spectral band width and chopped light waveform. In: *Conference Record of the Twenty Sixth IEEE Photovoltaic Specialists Conference - 1997*. IEEE; 1997:471-474. doi:10.1109/PVSC.1997.654130

42. Moraitis P, Leeuwen G, Sark W. Visual Appearance of Nanocrystal-Based Luminescent Solar Concentrators. *Materials*. 2019;12(6):885. doi:10.3390/ma12060885

43. *Impact of UV Radiation on Genome Stability and Human Health*.

44. Sark WGJHMV, Barnham KWJ, Slooff LH, et al. Luminescent Solar Concentrators - A review of recent results. *Opt Express*. 2008;16(26):21773. doi:10.1364/OE.16.021773

45. Stefania Castelletto, Alberto Boretti. Luminescence solar concentrators: A technology update. doi:https://doi.org/10.1016/j.nanoen.2023.108269

46. Damon M. de Clercq a, Sanutep V. Chan a, Jake Hardy a, Michael B. Price a b c, Nathaniel J.L.K. Davis. Reducing reabsorption in luminescent solar concentrators with a self-assembling polymer matrix. doi:https://doi.org/10.1016/j.jlumin.2021.118095

47. Ren TB, Xu W, Zhang W, et al. A General Method To Increase Stokes Shift by Introducing Alternating Vibronic Structures. *J Am Chem Soc*. 2018;140(24):7716-7722. doi:10.1021/jacs.8b04404

48. Puttavva Meti a, Fahad Mateen b, Do Yeon Hwang b, Ye-Eun Lee b, Sung-Kyu Hong b, Young-Dae Gong. Luminescent solar concentrator based on large-Stokes shift tetraphenylpyrazine fluorophore combining aggregation-induced emission and intramolecular charge transfer features. doi:https://doi.org/10.1016/j.dyepig.2022.110221.

49. Stokes shift - Wikipedia. Accessed May 1, 2024. https://en.wikipedia.org/wiki/Stokes_shift

50. Shujun Wang, Lihong Gao. *Chapter 7 - Laser-Driven Nanomaterials and Laser-Enabled Nanofabrication for Industrial Applications*.

51. Properties, synthesis, and applications of carbon dots: A review. doi:https://doi.org/10.1016/j.cartre.2023.100276

52. Xiangcao Li a, Yanzhao Fu a, Shaojing Zhao a, JiaFu Xiao d, Minhuan Lan a, Benhua Wang a, Kui Zhang c, Xiangzhi Song a, Lintao Zeng. Metal ions-doped carbon dots: Synthesis, properties, and applications.

53. Nguyen KG, Baragau IA, Gromicova R, et al. Investigating the effect of N-doping on carbon quantum dots structure, optical properties and metal ion screening. *Sci Rep*. 2022;12(1):13806. doi:10.1038/s41598-022-16893-x

54. Timur Sh. Atabaev I. Doped Carbon Dots for Sensing and Bioimaging Applications: A Minireview. doi:10.3390/nano8050342

55. Sheng-Tao Yang, Xin Wang, Haifang Wang, Fushen Lu, Pengju G. Luo, Li Cao, Mohammed J. Meziani, Jia-Hui Liu, Yuanfang Liu, Min Chen, Yipu Huang,Ya-Ping Sun. Carbon Dots as Nontoxic and High-Performance Fluorescence Imaging Agents. doi:10.1021/jp9085969

56. Hesam Salimi Shahraki a, Anees Ahmad a, Rani Bushra. Green carbon dots with multifaceted applications– Waste to wealth strategy. doi:https://doi.org/10.1016/j.flatc.2021.100310

57. Bruno Peixoto de Oliveira a b, Flávia Oliveira Monteiro da Silva Abreu. Carbon quantum dots synthesis from waste and by-products: Perspectives and challenges.

58. Nair B. Final Report On the Safety Assessment of Polyvinylpyrrolidone (PVP).

59. Aleksandra Nešić a, Jovana Ružić a, Milan Gordić a, Sanja Ostojić b, Darko Micić b, Antonije Onjia. Pectin-polyvinylpyrrolidone films: A sustainable approach to the development of biobased packaging materials.

60. Nafiseh Kazemifard, Ali A. Ensafi, Behzad Rezaei. Green synthesized carbon dots embedded in silica molecularly imprinted polymers, characterization and application as a rapid and selective fluorimetric sensor for determination of thiabendazole in juices. doi:https://doi.org/10.1016/j.foodchem.2019.125812

61. Bhargav D. Mansuriya, Bhargav D. Mansuriya, SciProfilesScilitPreprints.orgGoogle Scholar, ORCID and Zeynep Altintas. Carbon Dots: Classification, Properties, Synthesis, Characterization, and Applications in Health Care—An Updated Review (2018–2021). doi:https://doi.org/10.3390/nano11102525

62. Heidari B, Salmani S, Sasani Ghamsari M, Ahmadi M, Majles-Ara MH. Ag/PVP nanocomposite thin film with giant optical nonlinearity. *Opt Quantum Electron*. 2020;52(2):86. doi:10.1007/s11082-020-2204-2

63. Liu M. Optical Properties of Carbon Dots: A Review. *Nanoarchitectonics*. 2020;1(1):1-12. doi:10.37256/nat.112020124.1-12

64. Khan WU, Wang D, Zhang W, et al. High Quantum Yield Green-Emitting Carbon Dots for Fe(III) Detection, Biocompatible Fluorescent Ink and Cellular Imaging. *Sci Rep*. 2017;7(1):14866. doi:10.1038/s41598-017-15054-9